Astronomy & Astrophysics manuscript no. neb1
June 6, 2016
©ESO 2016

arXiv:1606.01066v1 [astro-ph.SR] 3 Jun 2016

Atlas of monochromatic images of planetary nebulae *(Research Note)*

W. A. Weidmann[1, 2, ⋆], E. O. Schmidt[3], R. R. Vena Valdarenas[3], J. A. Ahumada[1], M. G. Volpe[1] and A. Mudrik[4]

[1] Observatorio Astronómico, Universidad Nacional de Córdoba, Laprida 854, 5000 Córdoba, Argentina
[2] Consejo Nacional de Investigaciones Científicas y Técnicas (CONICET)
e-mail: walter@oac.unc.edu.ar
[3] Instituto de Astronomía Teórica y Experimental (IATE), Universidad Nacional de Córdoba, CONICET, Observatorio Astronómico de Córdoba, Laprida 854, Córdoba, Argentina
[4] Facultad de Matemática, Astronomía y Física, Universidad Nacional de Córdoba

June 6, 2016

ABSTRACT

We present an atlas of more than one hundred original images of planetary nebulae (PNe). These images were taken in a narrow-band filter centred on the nebular emission of the [N II] during several observing campaigns using two moderate-aperture telescopes, at the Complejo Astronómico El Leoncito (CASLEO), and the Estación Astrofísica de Bosque Alegre (EABA), both in Argentina. The data provided by this atlas represent one of the most extensive image surveys of PNe in [N II]. We compare the new images with those available in the literature, and briefly describe all cases in which our [N II] images reveal new and interesting structures.

Key words. Planetary nebulae: General – Atlases – Catalogs – Stars: mass-loss

1. Introduction

Currently, about 3000 Galactic planetary nebulae (PNe) are known, which is more than twice as many as a decade ago; unfortunately, most of them still remain poorly studied. The PNe are highly representative of the latest stages of stellar evolution for stars of between 0.8 and 8 $M_{\odot}$; however, there are still many details of their evolutionary scheme such as the mass-loss processes, which are not yet fully understood. In this context, an extensive and complete atlas of narrow-band images centred on different nebular lines is essential because these images trace the distribution of ionized mass and also provide information about the processes of mass ejection involved in PN formation.

Clearly, it is important for any study about extended astronomical objects, and in particular for a study of PNe, to have access to a sample of narrow-band images that is as complete as possible. However, this type of work is time-consuming, which makes it an ideal project for medium-sized telescopes like those of the Complejo Astronómico El Leoncito (CASLEO) and the Estación Astrofísica de Bosque Alegre (EABA).

Despite the importance of these narrow-band surveys, there are not many works of this type. In addition, only a few studies contain observations in [N II] and in general cover only a small number of objects. The most relevant previous catalogues containing the [N II] narrow band that have been published are by Balick (1987, 50 objects), Manchado et al. (1996, 243 objects), Tweedy & Kwitter (1996, 19 objects), Hua et al. (1998, 22 objects), Górny et al. (1999, 101 objects) and Hajian et al. (2007, 18 objects).

Here we present an atlas of images comprising 108 PNe in the [N II] narrow band. The goal is to increase the amount of observational data of these amazing and highly complex objects. We hope that this work (together with the previous ones) will become a useful database for future research.

2. Sample, observations, and data reduction

We have observed a sample of 108 true PNe selected from the catalogues of Acker et al. (1992) and Parker et al. (2005). The selected nebulae did not have previous observations in [N II], except for a small group that was chosen to compare the quality of our data with that of previous works. Our selection criterion requires that the angular size of the objects in the mentioned catalogues be between 16 and 200 arcsec. In this way, it should be possible to infer its morphology and, in some cases, to detect low-ionization regions (LIS).

The observational data were obtained the 1.54 m telescope at EABA (configured in the newtonian focus) and the 2.15 m telescope at CASLEO. The imaging data for this survey were taken over the course of several observing runs from 2013 to 2015, making a total of 7 nights at CASLEO and 30 at EABA. The main features of the observational systems are described in Table 1. The transmission curves of the filters used are shown in Fig. 1.

In EABA, series of 20 consecutive six-minute exposures were obtained for most of the PNe. On the other hand, the lower brightness objects were observed at CASLEO where, in general, three exposures of ten minutes each were acquired. Some objects, such as He 2-15, were purposely oversaturated to show the faintest regions of the nebula. Table 4 summarizes our sample of objects, all of which were observed at low zenith distance ($z<40^{\circ}$).

⋆ Visiting Astronomer, Complejo Astronómico El Leoncito operated under agreement between the Consejo Nacional de Investigaciones Científicas y Técnicas de la República Argentina and the National Universities of La Plata, Córdoba and San Juan.

Table 1. Summary of the main features of the observational systems.

	EABA	CASLEO
telescope size [m]	1.54	2.15
f-ratio	4.9	8.6
CCD brand	Apogee	Roper
detector size [px]	3072×2048	2048×2048
binning [px]	3×3	5×5
pixel scale [arcsec/px]	0.74	0.75
field of view [arcmin]	12×8	5.1×5.1
central λ [Å][a]	6578	6582
bandpass filter [Å][a]	20	18
filter transmission $T_{\lambda 6585}$	0.92	0.53
zero-point k_0 [mag]	-3.38 ± 0.10	-1.77 ± 0.03
ext. coeff. k_1 [mag/airmass]	-0.08 ± 0.04	-0.11 ± 0.02
lim. magnitude [mag arcmin^{-2}]	12.1	12.6

Notes. The default gain for each instrument was used in all runs. [(a)] see Fig. 1.

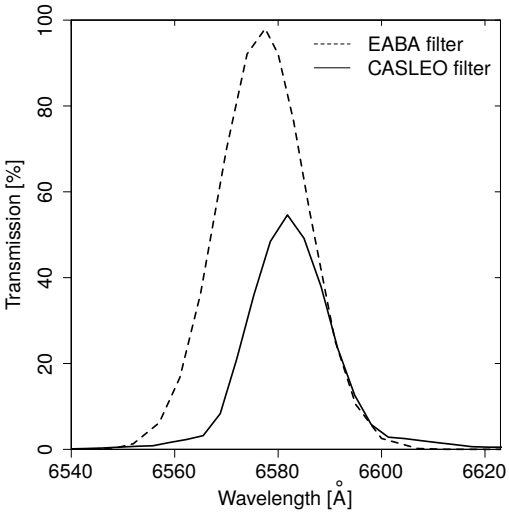

Fig. 1. Effective transmission curves for the filters (at 20 degrees Celsius).

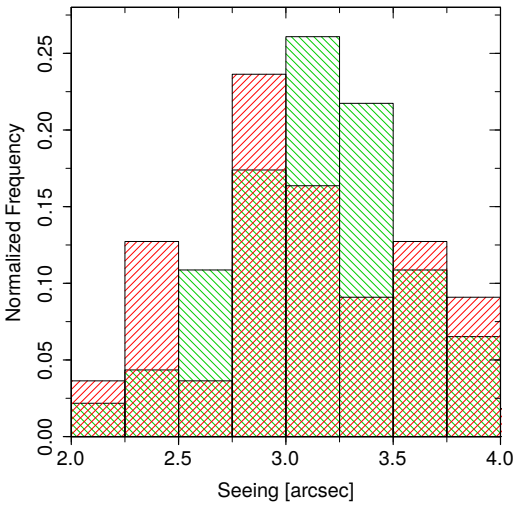

Fig. 2. FWHM of stars in CASLEO images, measured in the final combined frame (green) and individual reduced images (red).

Image reduction was performed using standard procedures with IRAF[1]. Thus, the data were first trimmed, bias-subtracted using a series of ten averaged bias frames and dark-subtracted (only in frames of EABA). The data were then flatfielded using a series of twilight flat fields. After the reduction was complete, the individual frames were spatially aligned to a common system using the IRAF task `imalign`. Typically, four stars were used to obtain this transformation. After that, all images were combined, cosmic rays removed, and the signal-to-noise (S/N) improved (IRAF task `imcombine`). Finally the images were rotated so that north was up and east to the left (IRAF tasks `imtranspose` and `rotate`).

The sky conditions during each night varied greatly. The combined effects of occasional poor telescope guiding and variable dome and sky seeing resulted in the stellar FWHM ranging from 2″ to 5″, as illustrated in Fig. 2 for CASLEO.

Moreover, since the final images suffered a slight degradation in quality due to the spatial alining process, this effect is shown in Fig. 2. The combined images with a seeing greater than 4″ were rejected. All the objects in the atlas have a $S/N > 4$. More details about the images that were obtained at EABA are reported in Vena Valdarenas et al. (2015).

2.1. Photometric calibration and detection limit

To assess the detection limit at each observatory, two additional nights were devoted to the observation of two planetary nebulae and of a number of spectrophotometric standard stars to first derive the extinction coefficients for the filters and the sensibility of the instrumental systems. The observed nebulae are *i)* the faint PN G242.5−05.9 (on the night of 15–16 October 2015 from CASLEO), and *ii)* the brighter PN G002.7−52.4 (IC 5148, on the night of 17–18 October 2015 from EABA). During each night, several secondary and tertiary spectrophotometric standard stars from Hamuy et al. (1994) were also observed at airmasses in the ranges 1.01–1.88 (CASLEO) and 1.01–1.41 (EABA). Exposures for the stars reach from a few to 180 seconds. Several images of 600 seconds of PN G242.5−05.9 at airmasses of ∼1.01, and of 360 seconds at ∼1.15 for PN G002.7−52.4 were obtained and combined to improve the S/N relation.

Aperture photometry was performed on nebulae and stars with the package DAOPHOT in IRAF. For standard stars, apertures with radii of four times the FWHM of the stellar images were adopted without recourse to aperture correction. For PN G242.5−05.9 an aperture of 30 arcsec of radius centred on $\alpha = 07^{\rm h}26^{\rm m}04\overset{\rm s}{.}9$, $\delta = -28°58'23\overset{''}{.}6$ (J2000.0) was used, and for PN G002.7−52.4 an aperture of 79 arcsec of radius centred on $\alpha = 21^{\rm h}59^{\rm m}35\overset{\rm s}{.}1$, $\delta = -39°23'07\overset{''}{.}1$ (J2000.0) was chosen. In the first case, four stars that appear inside the nebula and a fifth one very near its apparent limits were successfully subtracted before performing the photometry. No star was subtracted from IC 5148.

The transformation equations are of the form:

$$M(\lambda 6585) = m(\lambda 6585) + k_0 + k_1 \times X, \quad (1)$$

[1] IRAF: the Image Reduction and Analysis Facility is distributed by the National Optical Astronomy Observatories, which is operated by the Association of Universities for Research in Astronomy, Inc. (AURA) under cooperative agreement with the National Science Foundation (NSF).

Table 2. Adopted magnitudes at λ6585 of spectrophotometric standards.

Star	$M(\lambda6585)$
EG 21	11.936
HR 718	4.611
HR 1544	4.634
HR 9087	5.414
LTT 377	11.106
LTT 1020	11.320
LTT 2415	12.125

Table 3. Calibrated magnitudes and fluxes at λ6585 of two planetary nebulae.

	PN G002.7−52.4 (EABA)	PN G242.5−05.9 (CASLEO)
$M(\lambda6585)$	8.78 ± 0.04	14.20 ± 0.12
f_λ[a]	$(7.8 \pm 0.3) \times 10^{-13}$	$(5.2 \pm 0.6) \times 10^{-15}$
$\log f_\lambda$	-12.11 ± 0.04	-14.3 ± 0.1
surface brightness[b]	10.36 ± 0.05	12.56 ± 0.14
surface brightness[c]	$(5.0 \pm 0.6) \times 10^{-17}$	$(6.6 \pm 1.0) \times 10^{-18}$

Notes. [(a)] erg cm^{-2}s^{-1}Å^{-1}. [(b)] mag arcmin^{-2}. [(c)] erg cm^{-2}s^{-1}Å^{-1}arcsec^{-2}.

where $M(\lambda6585)$ is the calibrated monochromatic magnitude at λ6585, $m(\lambda6585)$ is the instrumental magnitude with an arbitrary zero point of 21.0, k_0 and k_1 are the zero-point and extinction coefficients, and X is the airmass. It is worth mentioning that the system sensitivity, including the effects of telescope optics and detector response, and the filter transmission at λ6585 ($T_{\lambda6585}$, listed in Table 3), are included in k_0. The values of $M(\lambda6585)$ for the observed spectrophotometric standards were obtained by interpolating in Tables 6 and 7 of Hamuy et al. (1994) and are listed in Table 2. The derived coefficients and their errors, as given by DAOPHOT, are given in Table 1. The monochromatic magnitudes of the nebulae are shown in Table 3; these are related to the flux density f_ν at λ6585 by

$$M(\lambda6585) = -2.5 \times \log_{10}(f_\nu) - 48.590, \quad (2)$$

(Hamuy et al. 1994), where f_ν is expressed in erg cm^{-2} s^{-1} Hz^{-1}. This flux density has to be multiplied by the factor $c/(6585)^2$ (c is the speed of light) to give it as f_λ, that is, in the units erg cm^{-2} s^{-1} Å^{-1}. After propagating the errors adequately, the flux densities of the nebulae and their logarithms are those listed in Table 3.

The surface brightnesses were calculated by adopting for circular shapes and areas of 0.217 arcmin^2 (PN G242.5−05.9) and 4.313 arcmin^2 (PN G002.7−52.4) for the nebulae. For the first, a surface brightness of 12.56 mag arcmin^{-2} at a S/N ∼ 4 for an exposure time of 600 seconds is estimated, while for IC 5148 the value is 10.36 mag arcmin^{-2} with S/N ∼ 20 and 360 seconds. These brightnesses, expressed in magnitudes per squared arcmin and also in erg cm^2 s^{-1} Å^{-1} arcsec^{-2}, are listed in Table 3. While the surface brightness of the faint nebula observed at CASLEO can be adopted as the limiting magnitude for the images taken there, IC 5148 is rather bright, therefore we divided its flux by 5 to obtain a S/N relation of ∼ 4 like that measured in a combination of 360-second exposures of the faint nebula Hf 39 (Figure 13). The magnitude calculated with this new flux, 12.1 mag arcmin^{-2}, can now be considered as the limiting magnitude in the images obtained at EABA for this survey.

It must be pointed out, finally, that the transformation derived in this section is in general not applicable to our collection of images, since observing on photometric nights was not a requirement for the original purposes of this work.

3. Considerations about the survey

3.1. Narrow-band filters

When interference filters are used in a converging beam, the primary effect is a shift of the transmittance peak towards shorter wavelengths (Eather & Reasoner 1969).

Another important phenomenon that affects our observations is the bandpass shift due to variations of the ambient temperature (Pogge 1992). It moves towards the red or the blue, depending on whether the temperature increases or decreases, respectively, following a linear temperature dependence. For a narrow-band filter, the shift in mean wavelength due to temperature is about 0.18Å per degree Celsius. An additional problem is posed by the age of filters: after 6-10 years they usually deteriorate, mainly losing transmittance.

On the other hand, we have to take into account the radial velocity of the objects. The radial velocity of a PN could cause the [N II] emission to falls outside of the effective bandpass of the filter. Unfortunately, many objects included in our atlas do not have radial velocity determinations, in particular the objects extracted from the MASH catalogue (Parker et al. 2005).

The filter peak transmittance was determined at a temperature of 20°C, which means that those objects that were observed from EABA in winter (where the temperature may drop to 5°) and with positive radial velocity might be contaminated by Hα emission. These objects are labelled in Table 4, where we used the radial velocity data from Durand et al. (1998) as a reference.

Finally, it is necessary to consider another possible nebular emission in this wavelength range. Fortunately, there are only very few nebular lines (C II at 6578.05 and 6582.88Å) that could contaminate our data. Nevertheless, contamination by continuous nebular emission will always be present.

3.2. Comparison with other observations

Our work has objects in common with the catalogues of Balick (1987) and Hua et al. (1998). These objects are labelled in Table 4. With the former, the only nebula in common is NGC 2610, which we observed from EABA. In this case the Balick images are deeper.

Our atlas includes ten PNe that were observed by Hua et al. (1998). The comparison in this case is more difficult, since Hua used three different telescopes and we used two. However, the images of those PNe that were observed from CASLEO are of a quality and depth comparable to those obtained by Hua et al. (1998) (e.g. He 2-70 and K 1-3).

4. Notes on individual objects

PN G002.7−52.4: ring-like PN with an inner highly elongated elliptical ring with several irregularities in the brightness and an external round fainter nebulosity. More images can be found in Streicher (2010), Moreno et al. (1991), and Chu et al. (1987).

PN G003.1+02.9: Stanghellini et al. (1993a) classified this PN as irregular. We disagree with this classification because in our image we can see an elliptical structure with prominent jets. More images can be found in Miszalski et al. (2009), López

(2000), Zhang & Kwok (1998), Hajian et al. (1997), López et al. (1997), and Corradi et al. (1996).

PN G013.8−02.8: bipolar PN. More images can be found in Saurer & Weinberger (1987).

PN G014.8−25.6: faint nebulosity with no obvious symmetry.

PN G019.4−13.6: middle elliptical according to the morphological scheme of Balick (1989). More images can be found in Bohigas (2003).

PN G043.5−13.4: PN with no clear symmetry, roughly elliptical with a nearly rectangular shape. More images can be found in Schwarz et al. (1992).

PN G118.8−74.7: a bright and well-studied object. Phillips (2003) classified this PN as round. Our image shows that it has an elliptical shape with an inner filamentary structure and intense patches to the SE. We suggest that the object needs to be reclassified. Images of this object are found in Pereyra et al. (2013), Chu et al. (2009), Hoogerwerf et al. (2007), Moore (2007), Szentgyorgyi et al. (2003b), and Szentgyorgyi et al. (2003a).

PN G209.1−08.2: in the MASH images the object is very faint and does not reveal any morphology. In our image it shows a clearly round morphology, with non-uniform brightness.

PN G215.6+11.1: curious morphology, nebula with a nearly rectangular shape. Possible bipolar PN.

PN G217.2+00.9: probable interaction with the ISM.

PN G224.3−03.4: probable interaction with the ISM.

PN G225.4+00.4: intriguing morphology, it displays a non-concentric multishell, similar to the mysterious rings of supernova 1987A.

PN G226.7+05.6: all authors agree that the object shows a bipolar morphology. Stanghellini et al. (1993b) classified it as bipolar with an outer structure. More images can be found in Huggins et al. (2000), Perinotto & Corradi (1998), Corradi & Schwarz (1995), Schwarz (1992), Schwarz et al. (1992), and Corradi & Schwarz (1993a).

PN G233.0−10.1: ring-like PN. More images can be found in Saurer & Weinberger (1987).

PN G236.0−10.6: object poorly studied, morphology type one-side (see Ali et al. 2000) with radial filaments. More images can be found in Hartl & Weinberger (1987).

PN G236.7−01.6: our image shows two areas of lower brightness that are not visible in the Hα image of the MASH catalogue.

PN G239.6−12.0: round with internal structure and intense patches. More images can be found in Fredrick & West (1984).

PN G239.6+13.9: Balick (1989) classified this PN as elliptical (early-middle subtype). Additional images can be found in Schwarz et al. (1992).

PN G243.8−37.1: Boffin et al. (2012a) performed a morphological analysis of this PN.

PN G247.5−04.7: there is an HII region towards the SW, and it is unclear whether it is part of the PN or is the optical counterpart of the molecular cloud BRAN 63.

PN G249.3−05.4: ring-like PN with a very faint CSPN. It shows several irregularities in the brightness of the ring.

PN G249.8+07.1: this seems to be two overlapping PN. It is difficult to explain the homogeneous and extensive overdensity of material towards the NW.

PN G250.4−01.3: classical bipolar PN with an arc towards the NW. It is also visible in the [N II] images of Kerber et al. (2000).

PN G257.5+00.6: poorly studied planetary nebula with intriguing morphology. The PN displays a ring-like structure of low surface brightness towards the NE and a emission region towards the SSE that is difficult to explain. It probably is a bipolar PN. This object requires a more detailed study.

PN G258.0−15.7: Gonçalves et al. (2002) show an [N II] image, but it is not as deep as ours. In both cases the huge jet-like features are clearly visible. Additional images can be found in Corradi et al. (1996) and Corradi et al. (1999).

PN G259.1+00.9: it is difficult to perform a morphological classification of this Type I PN. A complete analysis of this object was made by Jones et al. (2014). Our [N II] image does not show any differences with the [N II]+Hα published in that article. A Hα image is presented by Górny et al. (1999).

PN G260.7−03.3: the Hα image of MASH catalogue displays a more extended HII region than our image. According to its morphology, it would not be a PN. It could be a filament of the supernova remnant (SNR) Puppis A (Goudis & Meaburn 1978).

PN G261.6+03.0: Corradi & Schwarz (1995) classify this Type I PN as a possible/probable bipolar. Our [N II] image shows a well-defined bipolar morphology with a pronounced waist, thus we confirm this classification. It is not evident from our image if the two saturated regions define the torus of the waist. If this were the case, the waist would not be perpendicular to the bipolar lobes. To answer this question, it is necessary to perform a detailed spectroscopic study.

PN G261.9+08.5: this Type I PN has been classified by Peimbert & Torres-Peimbert (1983) as a filamentary bipolar. More images can be found in Vázquez (2012), Bohigas (2003) and Dufour (1984).

PN G262.6−04.6: it presents a roughly round shape with two intense oval patches. Additional images can be found in Longmore & Tritton (1980) and Schwarz et al. (1992).

PN G263.3−08.8: this object does not have published narrow-band images. Our image shows a round morphology with a dark band crossing the core, with a PA of 135°. Additional images can be found in Fredrick & West (1984).

PN G264.1−08.1: well-defined elliptical nebula with a high surface brightness and an evident central star.

PN G265.1−04.2: ring-like PN with some knots on the edge. It is unclear if the off-centre bright star is indeed its ionizing source. Additional images can be found in Fredrick & West (1984).

PN G265.4+04.2: round PN with two diametrically opposed condensations. Probable bipolar PN.

PN G268.6+05.0: object with no obvious symmetry. It displays an oval ring-like internal structure with opposite faint ansae. It might be a bipolar PN.

PN G268.9−00.4: this fascinating object has the appearance of a steering wheel. There is a nebulosity in the NW that is not visible in the MASH Hα image. It is unclear if it belongs to the nebula. The central bright star could be the ionizing source. This object deserves a more detailed study.

PN G274.6+03.5: round PN with a bright bar along its diameter. Additional images can be found in Górny et al. (1999).

PN G276.1−03.3: object that probably has a double envelope.

PN G277.1−03.8: López et al. (1989) have classified this PN as an evolved bipolar, but Louise et al. (1987) have classed it as peculiar. It has an overall bow-shock morphology, which was also noted by Rauch et al. (1999). Perhaps the gaseous envelope has interacted with the ISM. A detailed analysis of this object was presented by (Lopez et al. 1991). More narrow-band images can be found in Drew et al. (2014), Perinotto & Corradi (1998), Corradi & Schwarz (1995), and (Lopez et al. 1991).

PN G277.7−03.5: a round morphology with a complex ionization structure was revealed in our image. This object deserves a more detailed study.

PN G278.5−04.5: this object has been very poorly studied. Our image shows an elliptical envelope with an internal structure of point-symmetric type. In addition, we observe two pairs of beams in the E-W direction, similar to those of the Egg nebulae.

PN G279.1−03.1: roughly elliptical with two knots diametrically opposed.

PN G279.6−03.1: bipolar (Corradi & Schwarz 1995), intense knots are superimposed at each end of the minor axis. In addition, it has a pair of arcs that make it an S-shaped nebula (Lee et al. 2007b). A detailed study of this object has been made by Corradi & Schwarz (1993b). More images can be found in Lee et al. (2007a), Perinotto & Corradi (1998) and Schwarz et al. (1992).

PN G280.0+02.9: round or point-like nebula. We do not detect any outer structure.

PN G285.5−03.3: strange morphology for a PN. Perhaps it is indeed the galaxy LEDA 2792457 and/or LEDA 2792455.

PN G286.3−00.7: Smith et al. (2007) showed a [N II]+Hα narrow-band image of this PN. It is a clear ring PN.

PN G286.3+02.8: ring-like PN with a bright condensation to the SW.

PN G288.4−01.8: bipolar, it seems that its waist is a torus.

PN G288.4+00.3: it probably has two symmetrical jets at PA 100°.

PN G288.9−00.8: possible WR star of population I (Smith et al. 1994). Additional images can be found in Stahl (1987) and Frew et al. (2014).

PN G290.1−00.4: clear bipolar morphology with an bright waist. Moreover, in our image two ansae perpendicular to the minor axis are evident, which are not clear in the image published by Hua et al. (1998).

PN G290.5+07.9: the central star is visible. Well-studied object (see Palmer et al. 1996; Lopez et al. 1993), deeper images can be found in Boffin et al. (2012b).

PN G292.6+01.2: very bright PN with a complex internal structure. Bipolar appearance with a faint external shell. More images can be found in Górny et al. (1999).

PN G293.6+01.2: possible bipolar, with a very brilliant waist.

PN G293.6+10.9: well-defined irregular disc with a central hole. A double-shell structure can be seen. Aditional images can be found in Rauch et al. (1999).

PN G294.6+04.7: very complex object that has been studied in detail. It shows jets and knots (Corradi et al. 1999), an extended halo (Corradi et al. 2003, 2004), and a bow-shock feature (Guerrero et al. 2013). Additional narrow-band images can be found in Schwarz et al. (1992) and Richer et al. (1991).

PN G294.9−00.6: round morphology, an exterior elliptical structure may be present (PA=0°). The central region is probably obscured by dust.

PN G296.6−20.0: elliptical morphology that resembles the Owl nebula.

PN G298.2−01.7: Corradi & Schwarz (1995) classified it as a probable or possible bipolar PN. Our image allows us to confirm this classification. More images can be found in Górny et al. (1999).

PN G299.0+03.5: roughly elliptical with a bright waist. The central star is evident.

PN G299.0+18.4: ring-like with a diffuse double-shell; the central star is visible. Additional narrow-band images can be found in Schwarz et al. (1992).

PN G302.6−00.9: object poorly studied even though it displays a curious morphology. The PN exhibits an elliptical ring-like main structure. It seems to have a pair of symmetric jets in PA=135°.

PN G304.2+05.9: a ring-like object with a strange arc towards the NW. This is a very poorly studied object, it requires a more detailed analysis.

PN G307.2−03.4: PN with a puzzling morphology and a very hot [WO1] central star. Phillips & Reay (1983) reported five sets of ansae, but Reay et al. (1984) described this situation as a ring of condensations. Zuckerman & Aller (1986) classified this PN as irregular (with condensations and filaments), but Corradi & Schwarz (1995) classified it as a probable or possible bipolar PN and Pascoli (1990) as a late butterfly. Finally, Sabin et al. (2012) performed a detailed study of this object and classified it as a quadrupolar nebula with multiple sets of symmetrical condensations. Moreover, a spherical halo is evident in the [O III] image presented by Hua et al. (1998). In our image we can distinguish two mass-loss events. The first is an irregular structure of intense knots, and the other is an internal and discontinuous bar. More images can be found in Górny et al. (1999), Polcaro et al. (1997), Perinotto et al. (1994), and Greve & van Genderen (1987).

PN G309.0−04.2: we agree with the morphological description of Stanghellini et al. (1993a), who classified it as an elliptical with internal structure. Moreno et al. (1991) reported a nebulosity to the NW that we do not see. More images can be found in Kaler et al. (1989) and Schwarz et al. (1992).

PN G309.2+01.3: this PN is interacting with the ISM (Ali et al. 2012).

PN G310.7−02.9: narrow-band images are provided in Górny et al. (1999) and Moreno et al. (1991).

PN G310.8−05.9: round PN. More narrow-band images are shown in Longmore & Tritton (1980).

PN G311.7−00.9: bipolar, the waist looks like a torus. The central star is evident.

PN G315.0−00.3: the Hα image from Górny et al. (1999) shows a condensation towards the NW that is not visible in our image. Other images are presented by Moreno et al. (1991), Meaburn & Walsh (1989), and Moreno et al. (1987).

PN G317.1−05.7: the MASH Hα image shows an external envelope that is not visible in ours. On the other hand, the Hα image (Moreno et al. 1991) does not reveal the internal structure that appears in our [N II] image. In the [O III] image (Górny et al. 1999) none of these structures are visible. Other narrow-band images can be found in Moreno et al. (1987).

PN G317.8+03.3: poorly studied PN that presents a ring-like inner structure with several irregularities in the brightness. A diffuse nebulosity is superimposed at each end of the minor axis.

PN G318.3−02.0: all authors agree with the classsification of this PN as bipolar. More images can be found in Górny et al. (1999), Corradi & Schwarz (1995), Moreno et al. (1991), Louise et al. (1987), and Moreno et al. (1987).

PN G318.3−02.5: well-defined elliptical nebula with two intense patches. More images can be found in Górny et al. (1999), Moreno et al. (1991), and Moreno et al. (1987).

PN G318.4−03.0: ring-like PN.

PN G319.6+15.7: Type I PN with a [WR] core. This PN, according to its appearance, is a typical bipolar, but Zuckerman & Aller (1986) described this object as a disc of approximately uniform brightness, elliptical shape, and ansae. Hua et al. (1998) reported some internal structures. Several images of this PN have been taken in multiple works, for example O'Dell et al. (2002), Zhang & Kwok (1998), Corradi & Schwarz (1995), and Schwarz et al. (1992).

PN G321.8+01.9: ring-like type with a clear ansae to the W. Moreover, two symmetric condensations towards N and S are visible. We classify this object as a PE according to the classification scheme of Gorny et al. (1997). On the other hand, this PN has been classified as elliptical by Phillips (2003). Additional narrow-band images can be found in Górny et al. (1999).

PN G322.4−02.6: in the [N II]+Hα image published by Marston et al. (1998), the knots at the edge of the object towards the NW are not visible, but they are clear in our [N II] image and may be LIS. Hα and [N II] images shown by Schwarz et al. (1992) are overexposed. They do not show the complex internal structure that is evident in our [N II] image.

PN G327.8−07.2: the Hα image shows an elliptical ring of a faint nebulosity (Moreno et al. 1991). Our [N II] image is similar to the [O III] image of Moreno et al. (1991), showing a disc-like PN. In addition, a faint nebulosity to the N and S of the inner region is visible in both images.

PN G328.9−02.4: round PN, the diffuse nebulosity to the S that we see in our image is not visible in the [O III] images shown by Górny et al. (1999). It may be an ultracompact HII region (Walsh et al. 1997). There is a young stellar object candidate near to this object, reinforcing the hypothesis of an HII region.

PN G329.3−02.8: the Hβ image (Górny et al. 1999) does not show the two arcs (N and S) visible in our [N II] image. This structure could be a LIS. The central star is not at the geometric centre, probably because of an interaction with the ISM.

PN G331.5−03.9: elliptical shape with internal structures. Additional images can be found in Górny et al. (1999).

PN G332.0−03.3: round shape with several irregularities in the brightness. Additional images can be found in Górny et al. (1999).

PN G334.3−09.3: Gorny et al. (1997) classified this object as a bipolar PN, subclass BE, and we agree with this classification. On the other hand, Stanghellini et al. (1993a) classified it as elliptical with outer structure. The Hα image published by Schwarz et al. (1992) shows a round halo.

PN G340.8+10.8: diffuse nebulosity, elliptical shape. Two symmetric arcs are easily discernible superimposed at the edge of the nebula (PA=70°). This feature is not evident in the Hα image published by Górny et al. (1999).

PN G341.8+05.4: our image is different from the Hα image published by Górny et al. (1999), perhaps because of the seeing effects. It is difficult to perform a morphological classification, although it displays an elliptical shape (Gorny et al. 1997). We can distinguish in our image an internal structure. More images can be found in Liu et al. (2000) and Pottasch et al. (1986).

PN G342.7+00.7: it is probably a bipolar PN.

PN G342.9−02.0: the Hα image (Górny et al. 1999) displays a double-shell nebulosity. We can see in our [N II] image that there is an arc towards the S, still far away from the nebula.

PN G342.9−04.9: this object shows a morphology similar to PM 1-242 (Miranda et al. 2009). Additional images can be found in Górny et al. (1999).

PN G345.4+00.1: ring-like internal structure, with an external faint shell, intense condensations are superimposed towards the SE, and we can distinguish a knot towards the NE in our image. Stanghellini et al. (1993a) classified it as elliptical with an internal structure, Gorny et al. (1997) classified it as a probable elliptical. Additional images can be found in Schwarz et al. (1992).

PN G346.9+12.4: taking into account the peculiar morphology of this bright nebula, it is surprising that it has been very poorly studied. It consists of a bright ring-like internal structure with intense knots that are superimposed at each end of the minor axis. In addition, this object has an outer shell structure that is not perpendicular to the former. Hua et al. (1998) suggested that it is a bipolar PN, but we are unable to confirm this assertion.

PN G352.9+11.4: round PN with a [WCL] core. The morphology of this objects together with its brilliant CSPN make it similar to a nebula around a WC star of population I. Additional images can be found in Schwarz et al. (1992).

PN G353.7−12.8: this object could be the galaxy IRAS 18232−4031 according to its spiral morphology.

5. Results

The atlas of monochromatic images is presented in Figs. 3 to 20. In all the images we tried different brightness and contrast levels to emphasize the most interesting features of each object. A logarithmic scale is indicated with an "(L)" in the caption of the figures.

Our atlas includes objects that do not have any morphological classification (e.g. Wray 16−20, ESO 259−10, LoTr 7, and VBRC 6) or are very poorly studied (e.g. HaWe 9, SaWe 1, ESO 427−19, and ESO 209−15); in particular, it contains images of recently classified PNe (Parker et al. 2005). Moreover, this catalogue shows and reveals very interesting structures in several nebulae. For example, PHR0716−1053 displays a non-concentric multishell, resembling the mysterious rings of supernova 1987A, or the outstanding planetary nebulae VBRC 1 and Wray 16−121 that shows a capricious distribution of ionized material.

We compared our images with those available in the literature (even if they were taken in another filter), to compare our classification morphology with previous ones given by other authors. As a result, we reclassified some objects and provided one to those nebulae that did not have previous classification.

We hope that these new images and morphological descriptions presented here will provide a guide for future research, thus contributing to a better understanding of the final stages of stellar evolution.

Acknowledgements. We thank the referee, Romano Corradi, whose very useful remarks helped us to improve this paper. This work is partially supported by CONICET (PIP 11220120100298). The CCD and data ac-quisition system at CASLEO has been financed by R. M. Rich through U.S. NSF grant AST-90-15827. This work is partially based on observations obtained with the 1.54m telescope of the Estación Astrofísica de Bosque Alegre, dependent of the Universidad Nacional de Córdoba, Argentina. This research has made use of SAO Image DS9, developed by Smithsonian Astrophysical Observatory. This research made use of the SIMBAD database, operated at the CDS, Strasbourg, France.

References

Acker, A., Marcout, J., Ochsenbein, F., et al. 1992, The Strasbourg-ESO Catalogue of Galactic Planetary Nebulae. Parts I, II.
Ali, A., El-Nawawy, M. S., & Pfleiderer, J. 2000, Ap&SS, 271, 245
Ali, A., Sabin, L., Snaid, S., & Basurah, H. M. 2012, A&A, 541, A98
Balick, B. 1987, AJ, 94, 671
Balick, B. 1989, in IAU Symposium, Vol. 131, Planetary Nebulae, ed. S. Torres-Peimbert, 83–92
Boffin, H. M. J., Miszalski, B., & Jones, D. 2012a, A&A, 545, A146
Boffin, H. M. J., Miszalski, B., Rauch, T., et al. 2012b, Science, 338, 773
Bohigas, J. 2003, Rev. Mexicana Astron. Astrofis., 39, 149
Chu, Y.-H., Gruendl, R. A., Guerrero, M. A., et al. 2009, AJ, 138, 691
Chu, Y.-H., Jacoby, G. H., & Arendt, R. 1987, ApJS, 64, 529
Corradi, R. L. M., Manso, R., Mampaso, A., & Schwarz, H. E. 1996, A&A, 313, 913
Corradi, R. L. M., Perinotto, M., Villaver, E., Mampaso, A., & Gonçalves, D. R. 1999, ApJ, 523, 721

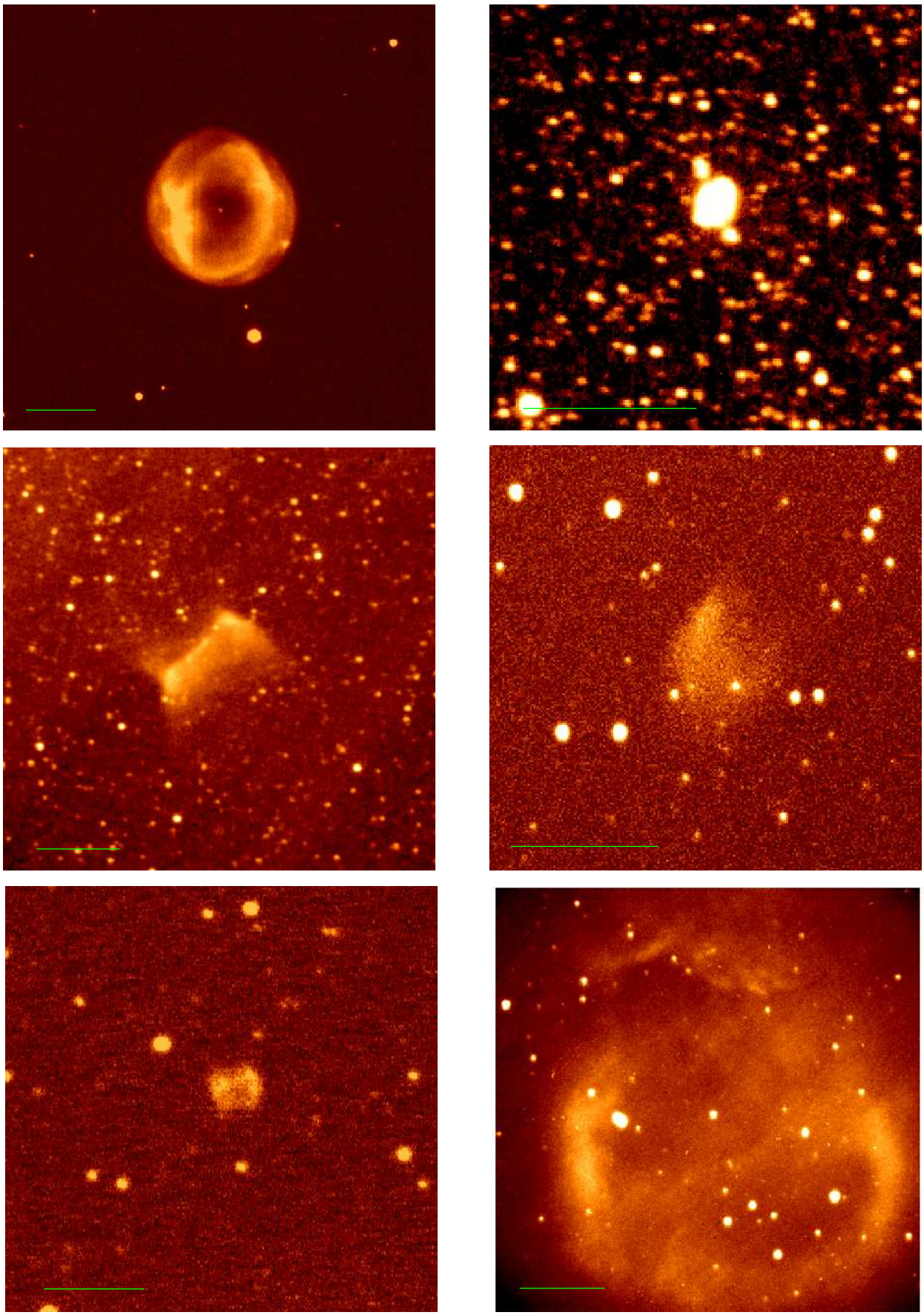

Fig. 3. [N II] images of planetary nebulae. North is up and east to the left. The scale is indicated by a bar representing 60 arcseconds. From left to right, top IC 5148−50 and Hb 4 (L), middle SaWe 3 and HDW 12, bottom DeHt 3 and A 66.

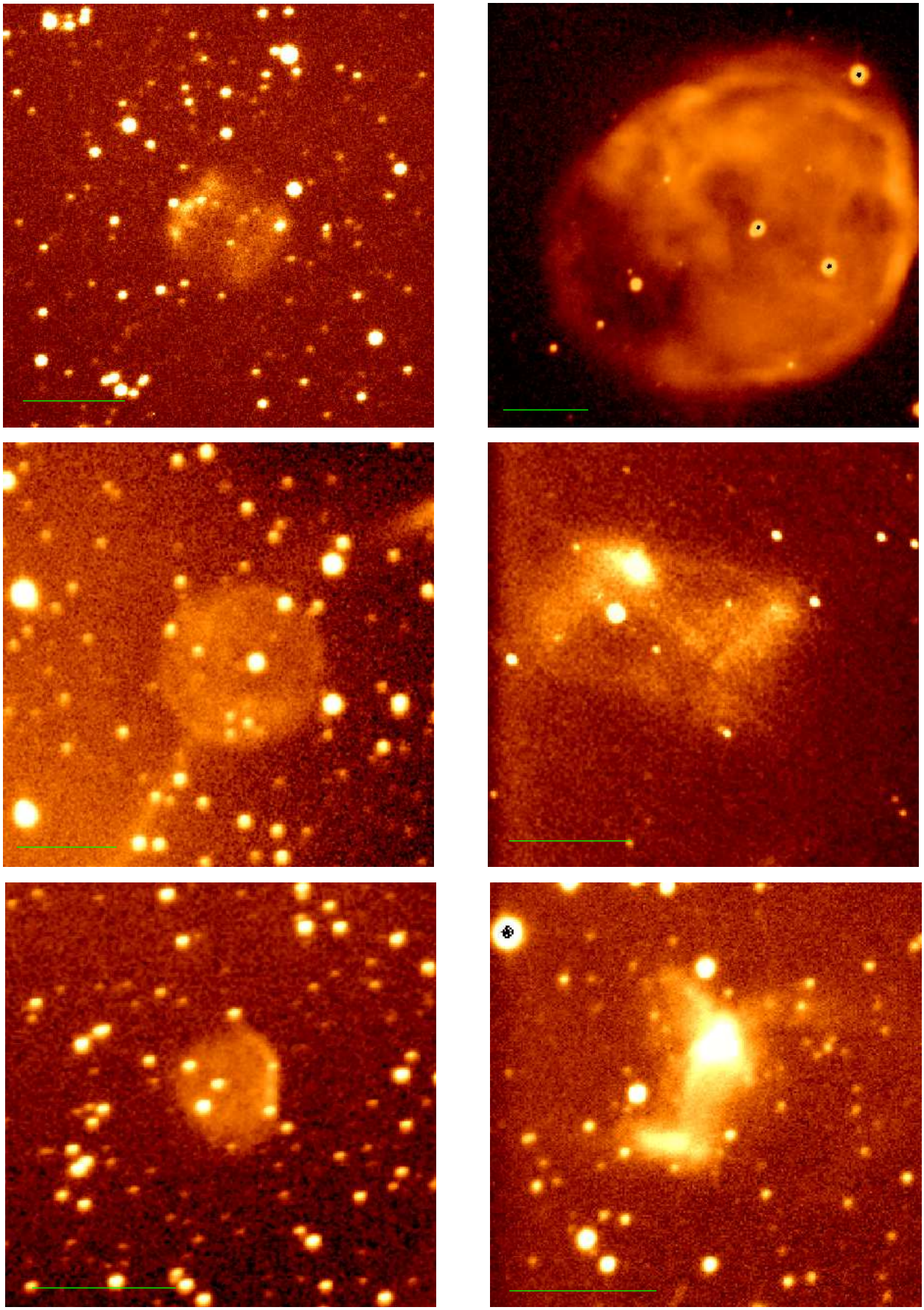

Fig. 4. Same as Fig. 3, top A 67 and NGC 246 (L), middle PHR0615−0025 (L) and K 1−11 , bottom PHR0702−0324 (L) and PHR0705−0924 (L).

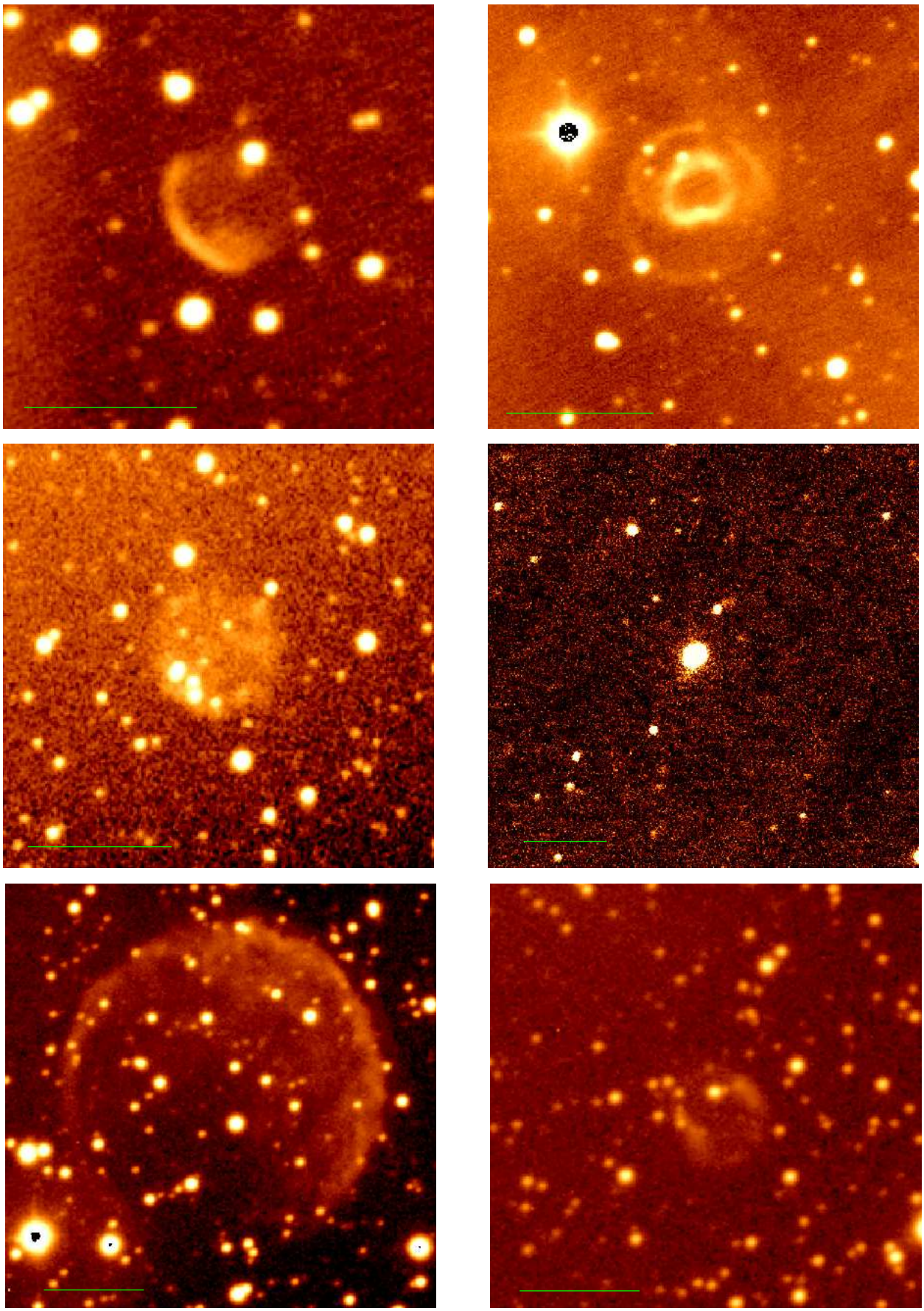

Fig. 5. Same as Fig. 3, top PHR0700−1143 (L) and PHR0716−1053, middle PHR0711−1238 (L) and M 1−6, bottom PHR0719−1222 (L) and PHR0727−1259 (L).

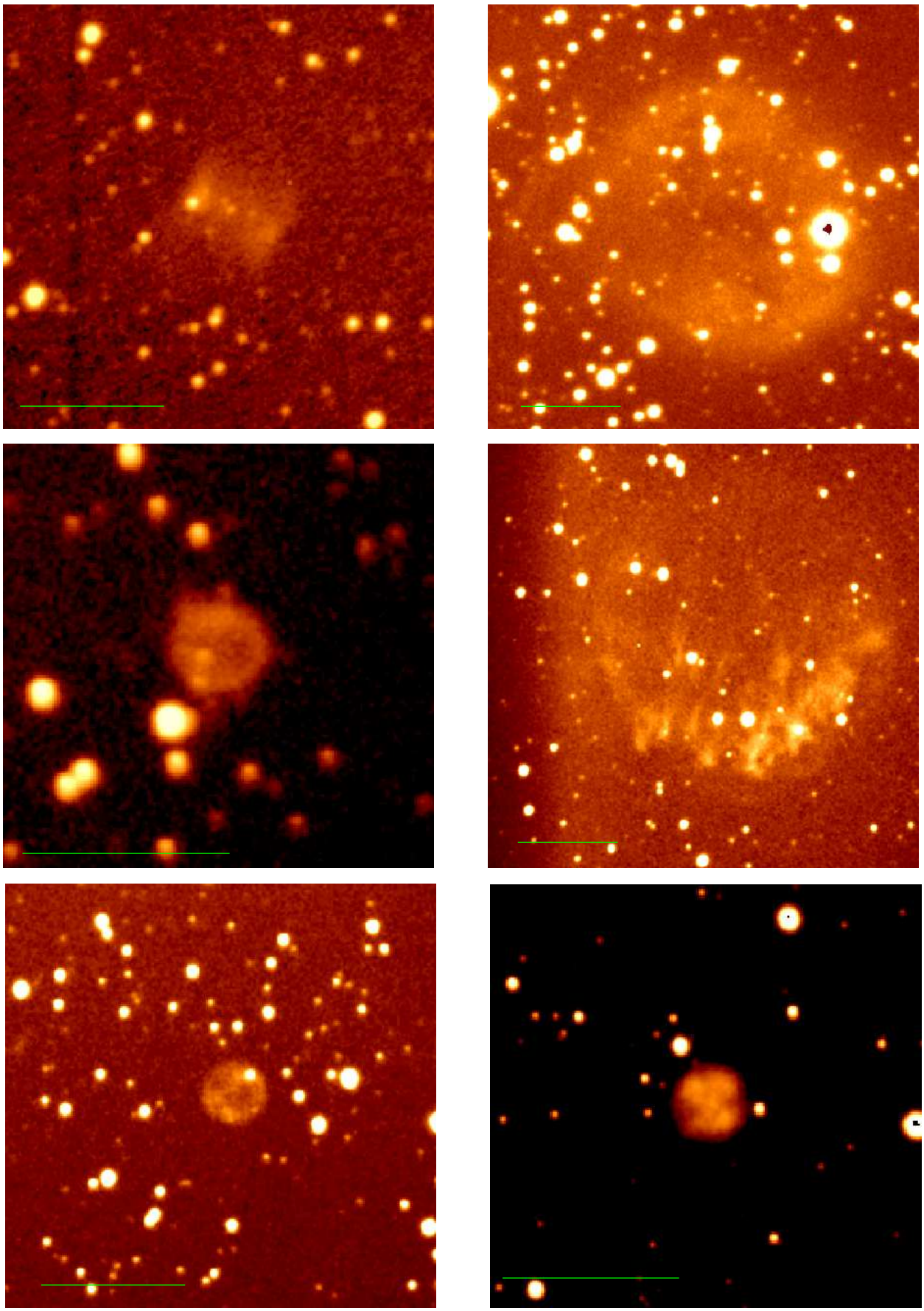

Fig. 6. Same as Fig. 3, top PHR0727−1707 (L) and PHR0724−1757, middle SaWe 1 and HaWe 9, bottom PHR0730−2151 and ESO 427−19 (L).

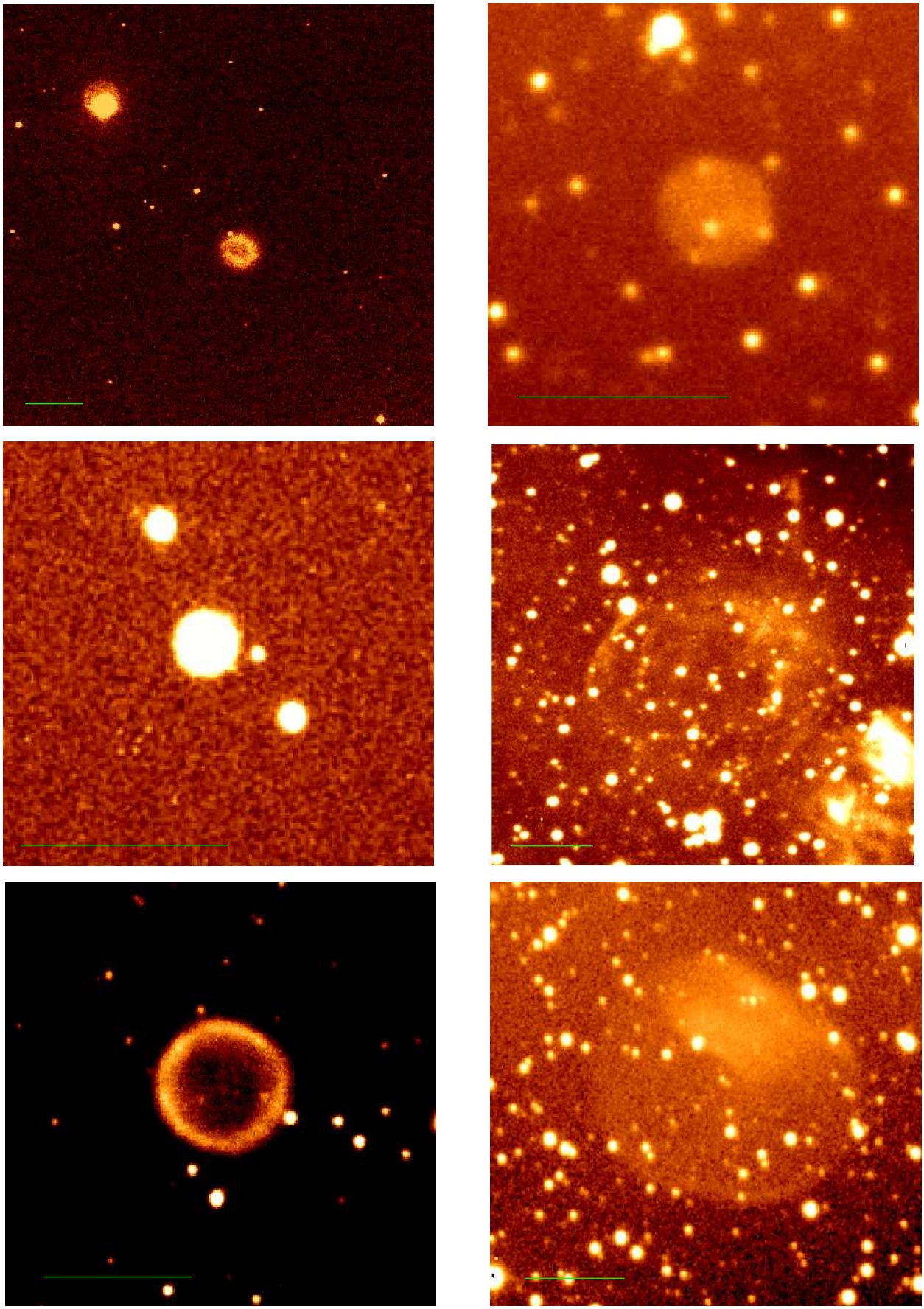

Fig. 7. Same as Fig. 3, top NGC 2610 and PHR0726−2858, middle PRTM 1 and PHR0742−3247, bottom A 23 and PHR0834−2819 (L).

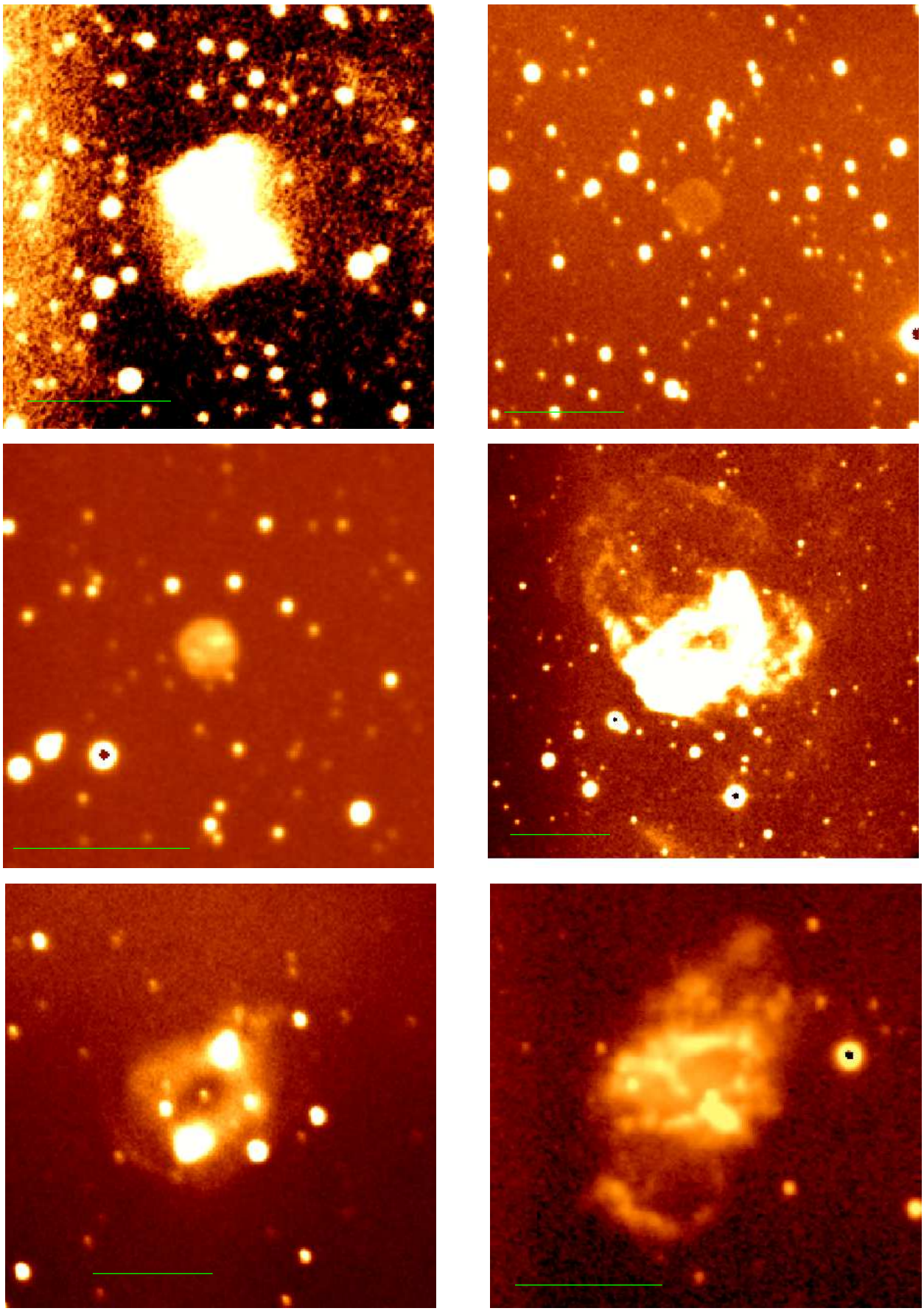

Fig. 8. Same as Fig. 3, top PHR0803−3331 (L) and PHR0736−3901, middle PHR0820−3516 and VBRC 1, bottom Wray 17−1 and He 2−11 (L).

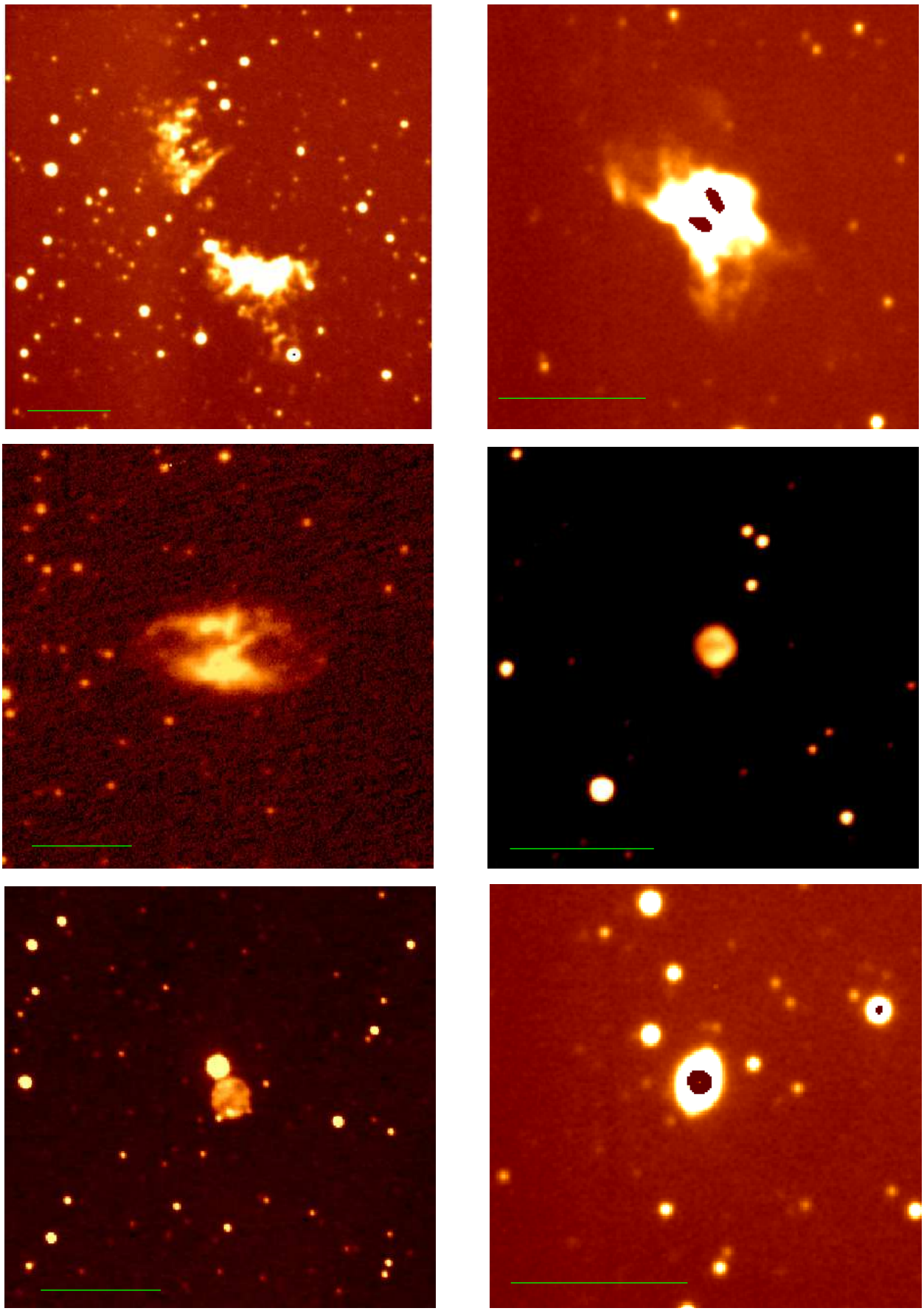

Fig. 9. Same as Fig. 3, top Wray 16−20 and He 2−15, middle NGC 2818 (L) and Wray 17−18 (L), bottom ESO 209−15 and He 2−7.

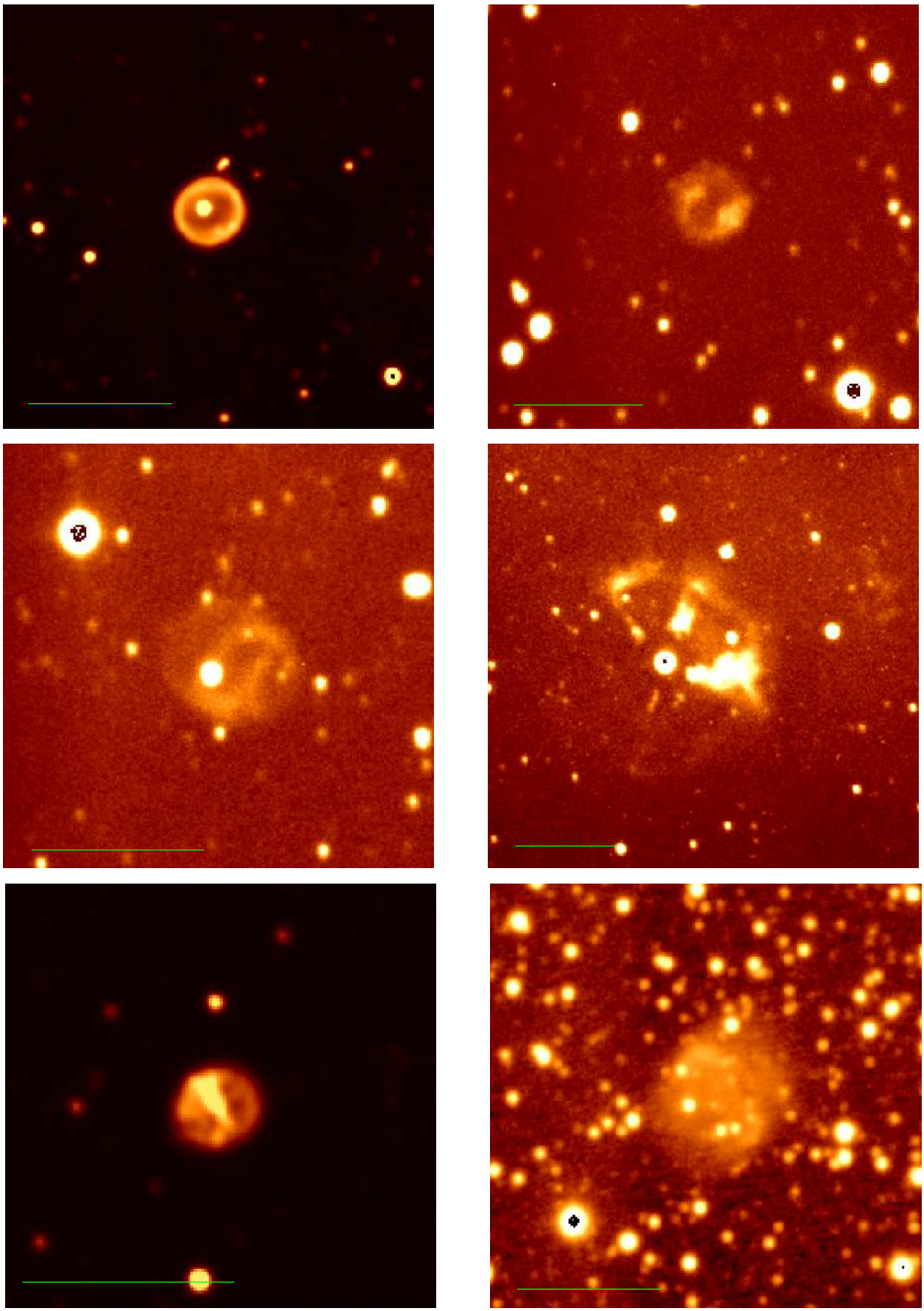

Fig. 10. Same as Fig. 3, top ESO 259−10 and PHR0911−4205, middle PHR0927−4347 and PHR0905−4753, bottom He 2−37 and PHR0924−5506.

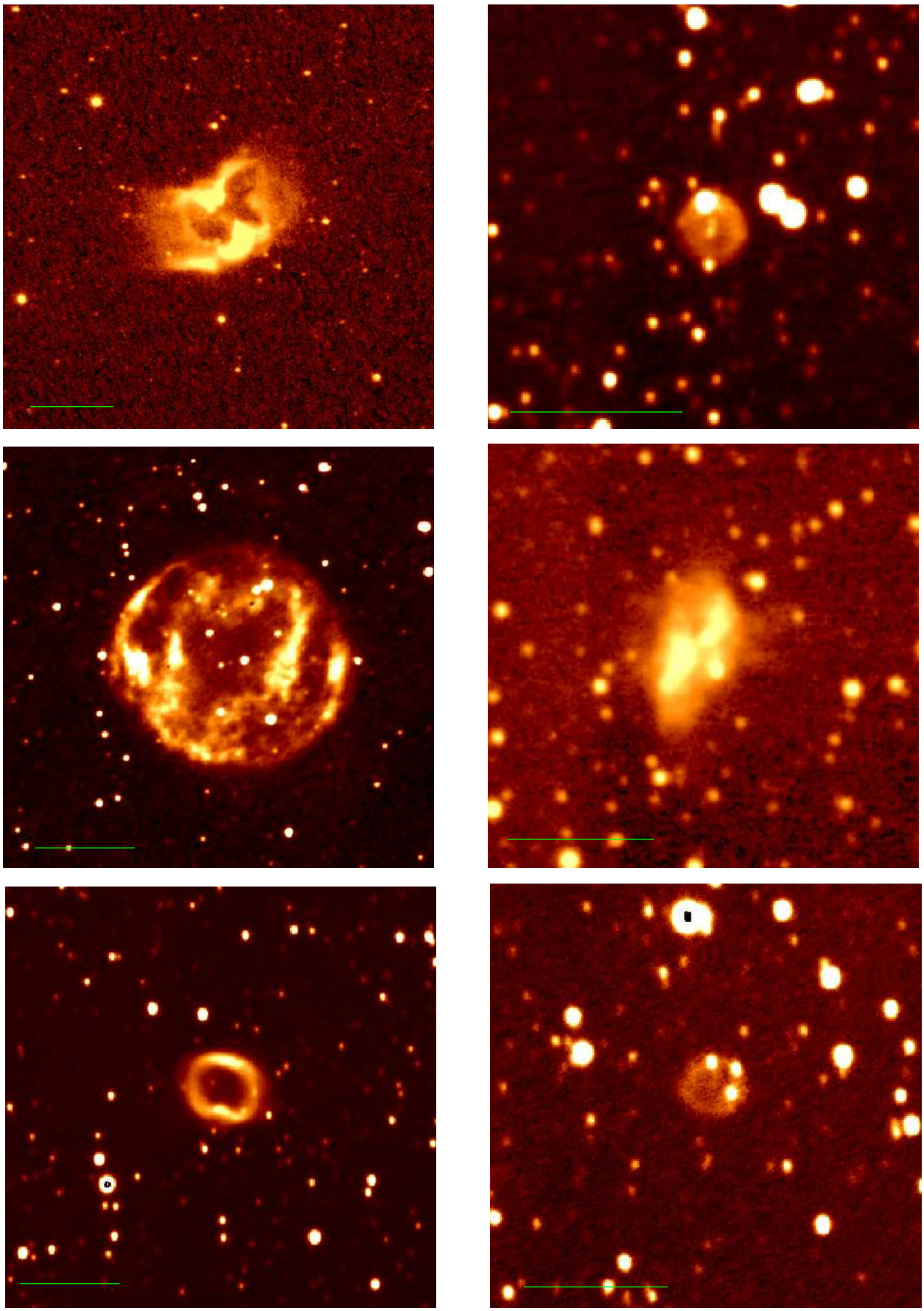

Fig. 11. Same as Fig. 3, top NGC 2899 (L) and PHR0958−5039, middle Wray 17−31 and He 2−32 (L), bottom PHR0940−5658 and PHR1010−5146.

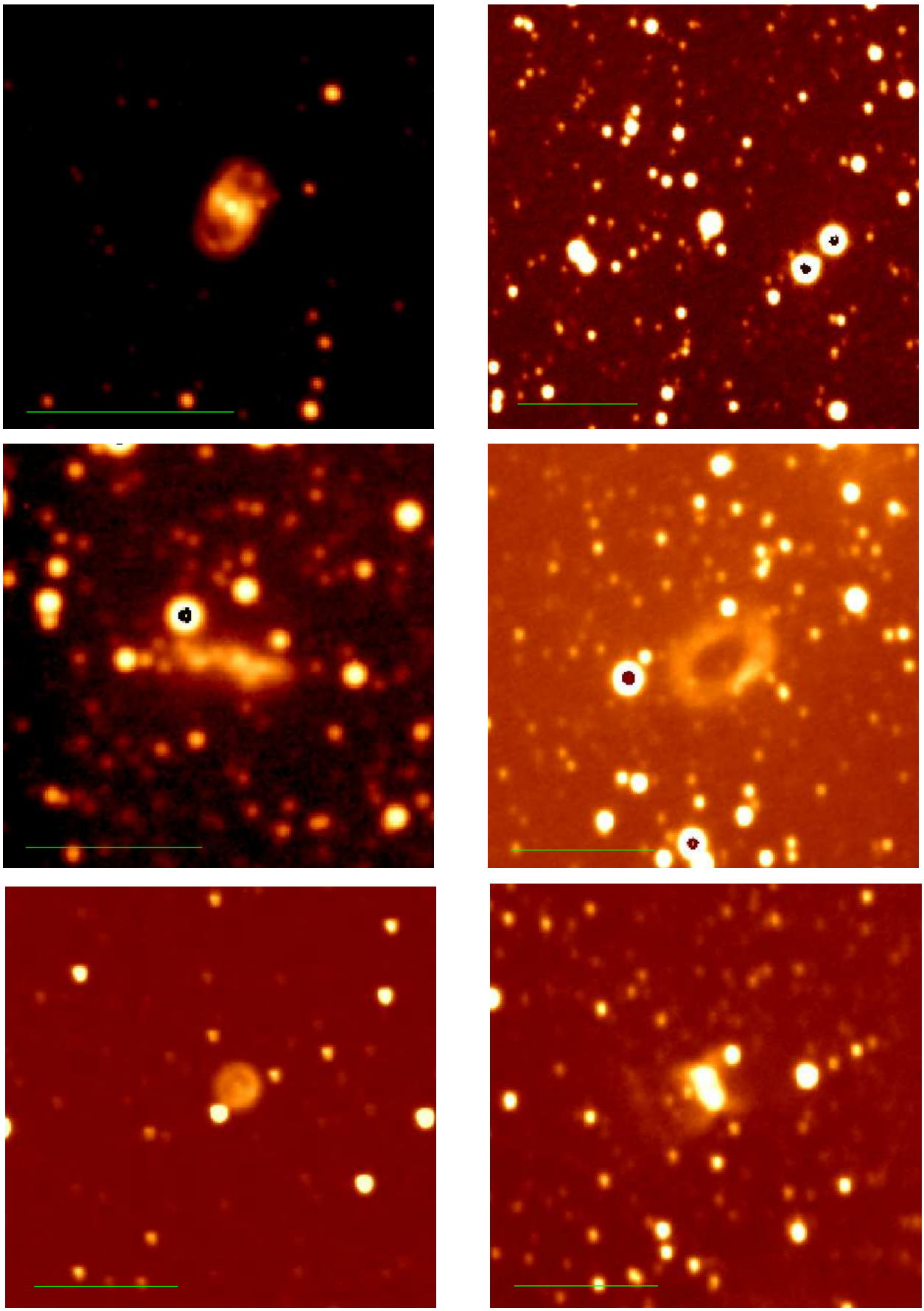

Fig. 12. Same as Fig. 3, top He 2−36 (L) and Ste 2−1, middle PHR1019−6059 (L) and PHR1036−5909, bottom He 2−55 and PHR1046−6109.

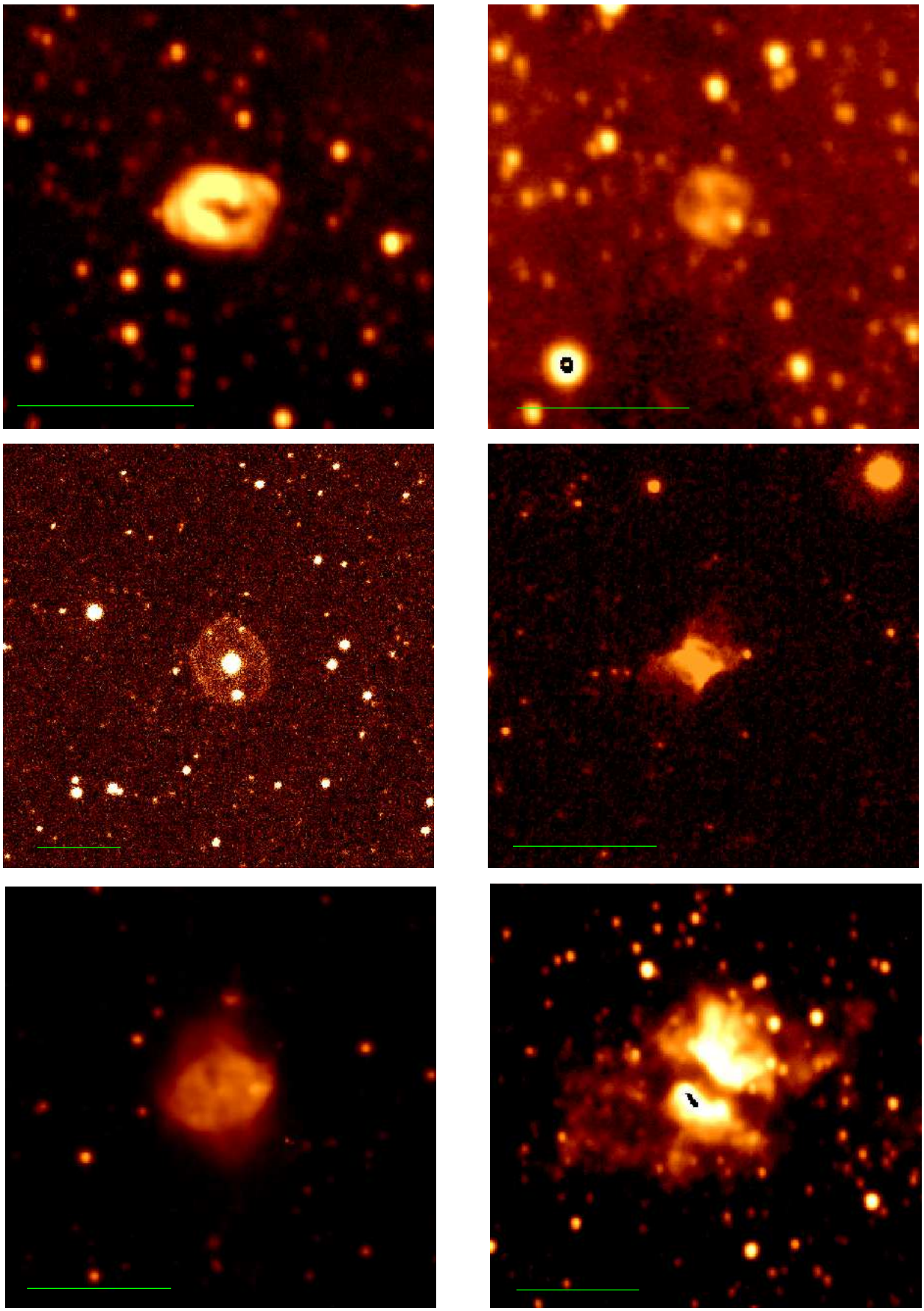

Fig. 13. Same as Fig. 3, top Hf 38 (L) and PHR1058−5853 (L), middle Hf 39 and Hf 48 (L), bottom Fg 1 (L) and NGC 3699 (L).

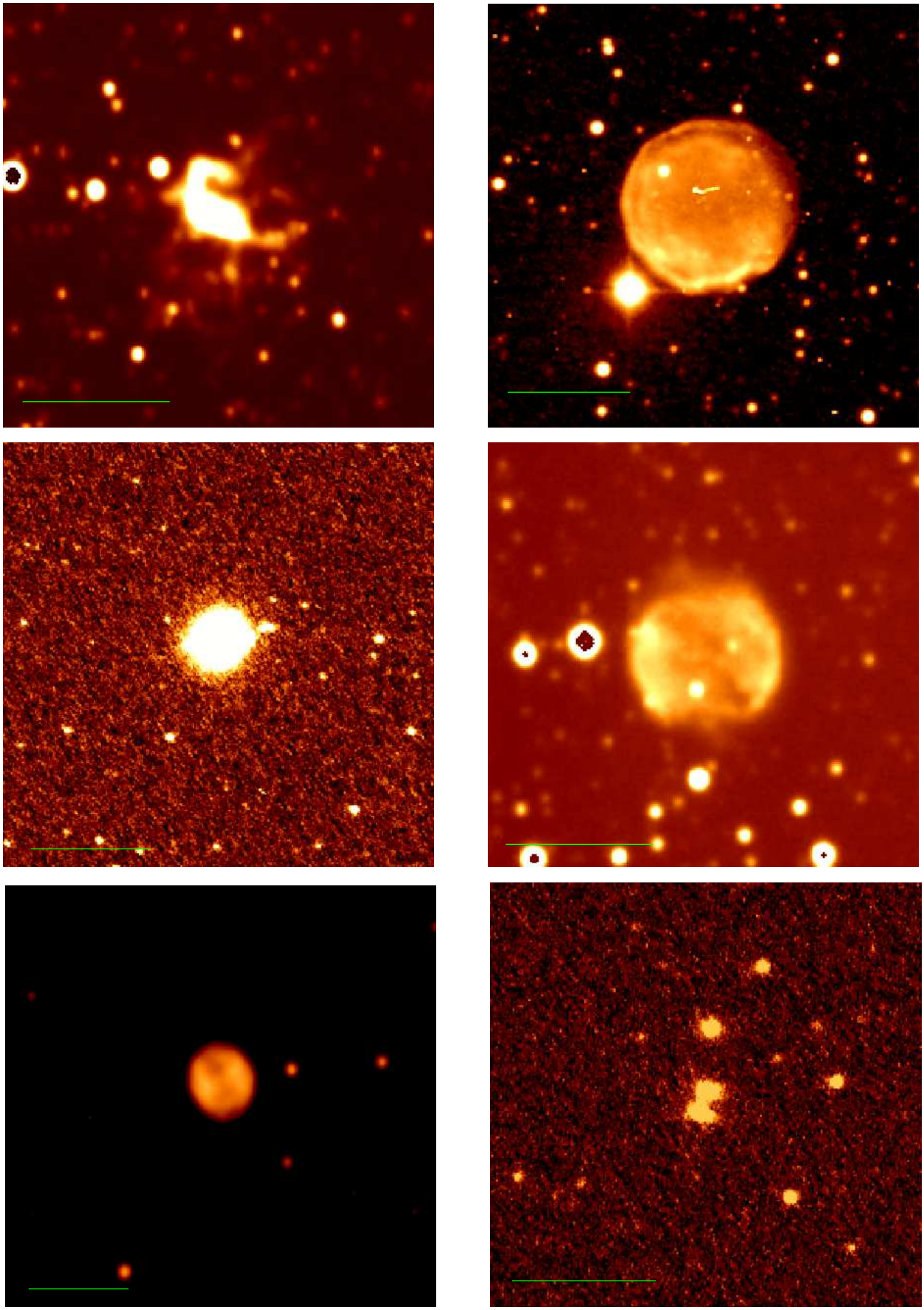

Fig. 14. Same as Fig. 3, top He 2−70 and BlDz 1, middle NGC 3918 and He 2−72, bottom NGC 3195 (L) and He 2-76.

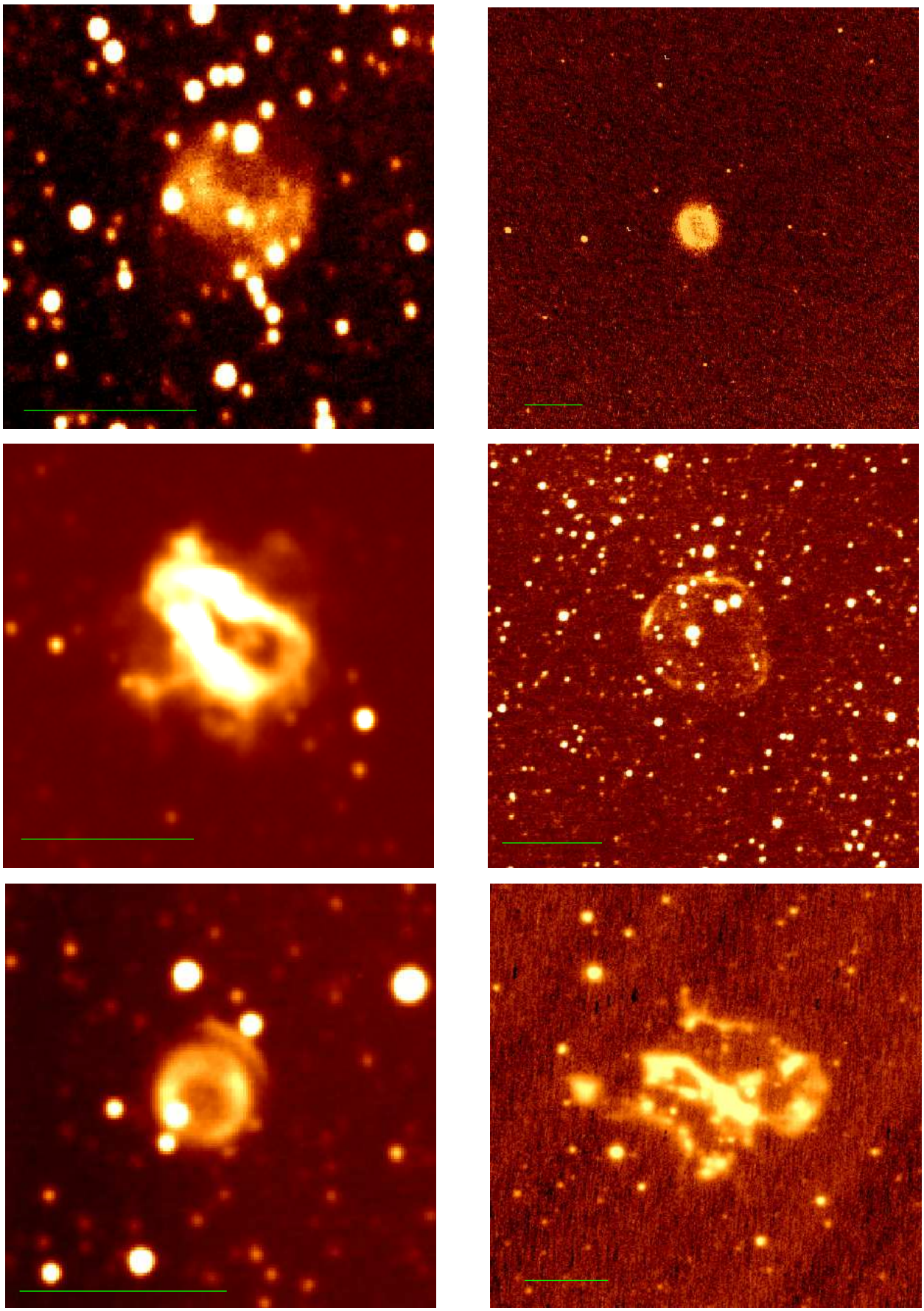

Fig. 15. Same as Fig. 3, top PHR1221−5907 and K 1−23, middle Wray 16−121, and PHR1250−6346, bottom Wray 16−122 and NGC 5189 (L).

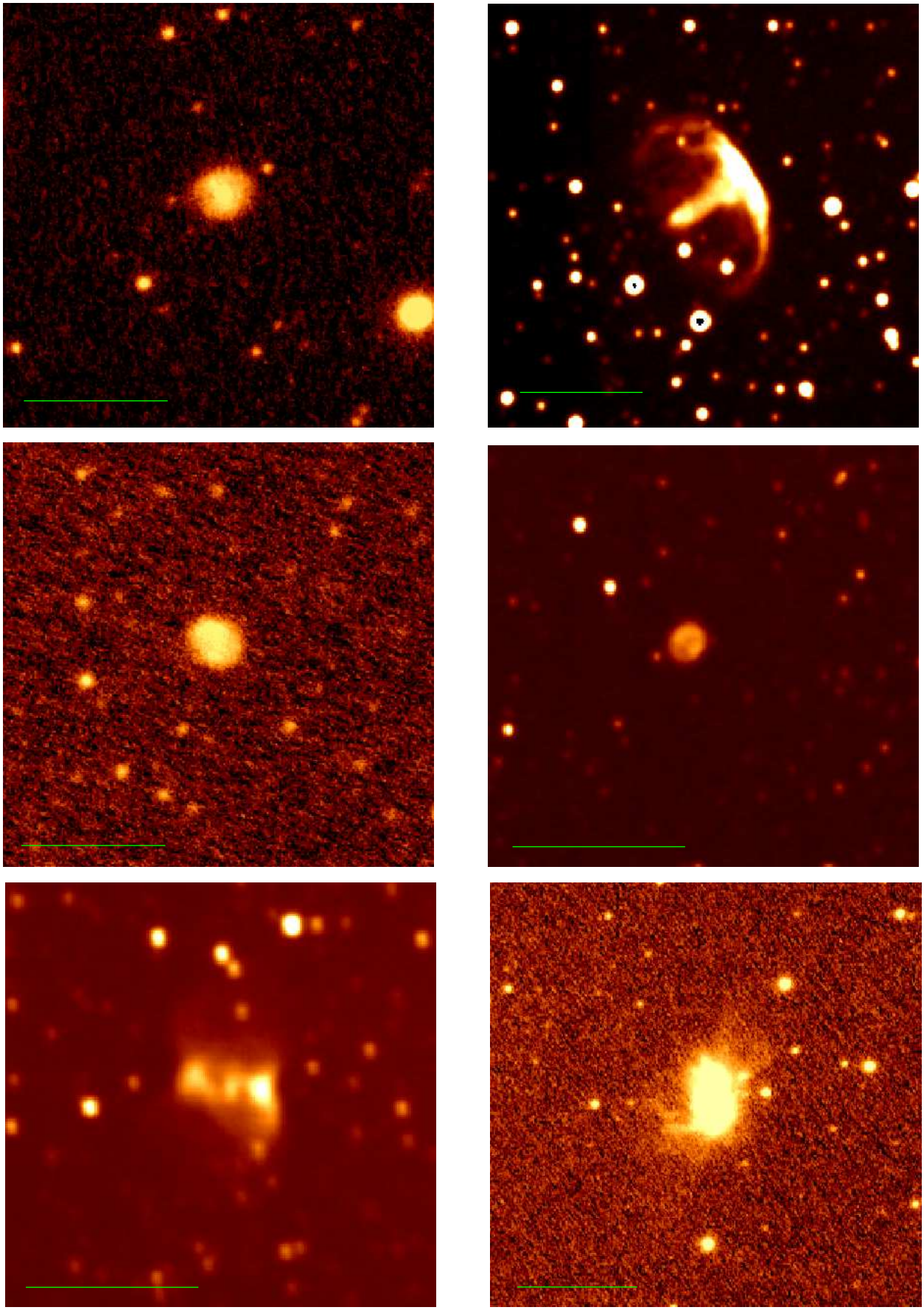

Fig. 16. Same as Fig. 3, top He 2−99 (L) and VBRC 5, middle He 2−103 (L) and LoTr 7, bottom PHR1408−6229, and He 2−111 (L).

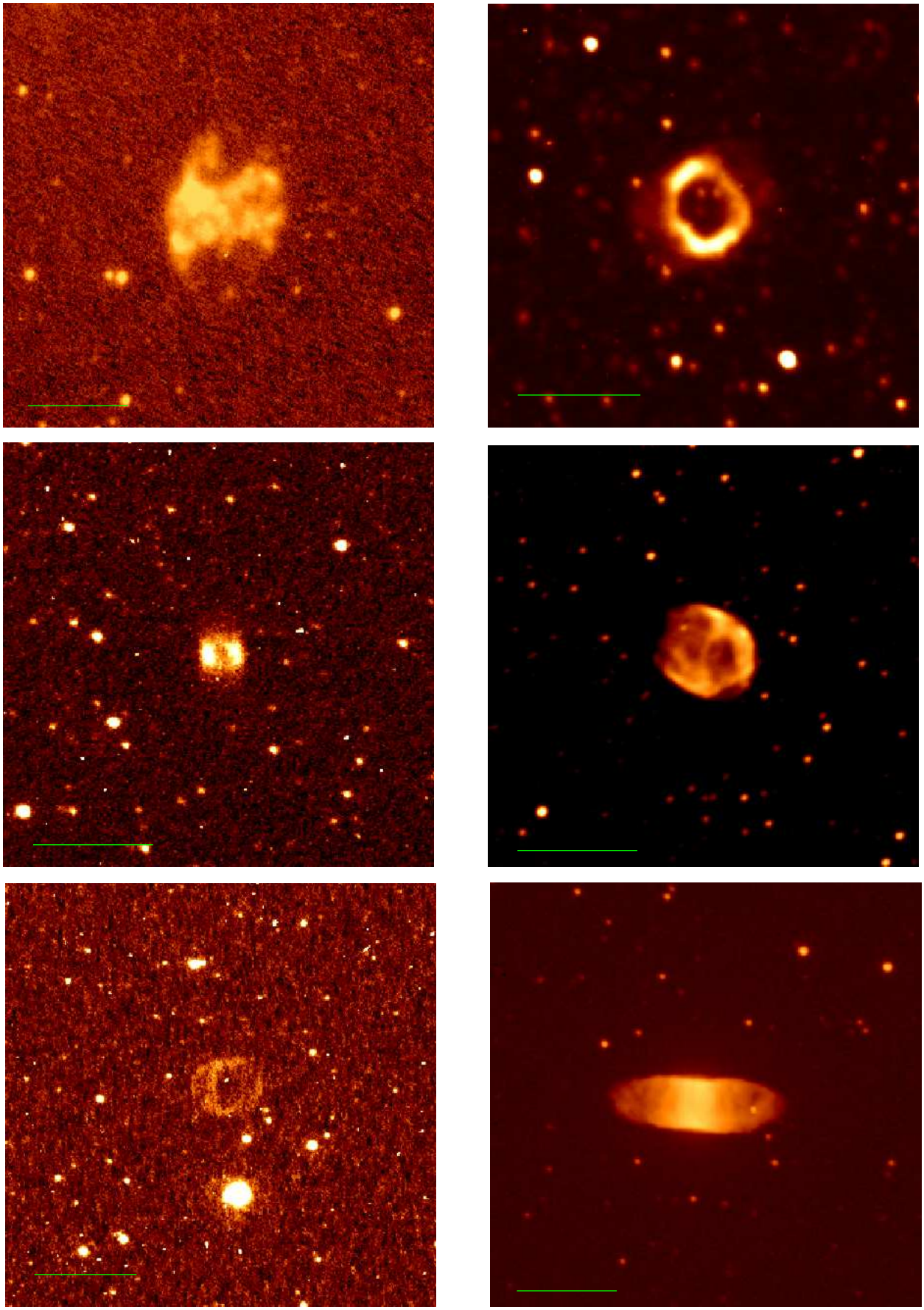

Fig. 17. Same as Fig. 3, top He 2−119 (L) and VBRC 6, middle He 2−114 and He 2−116 (L), bottom ESO 135−04 and IC 4406 (L).

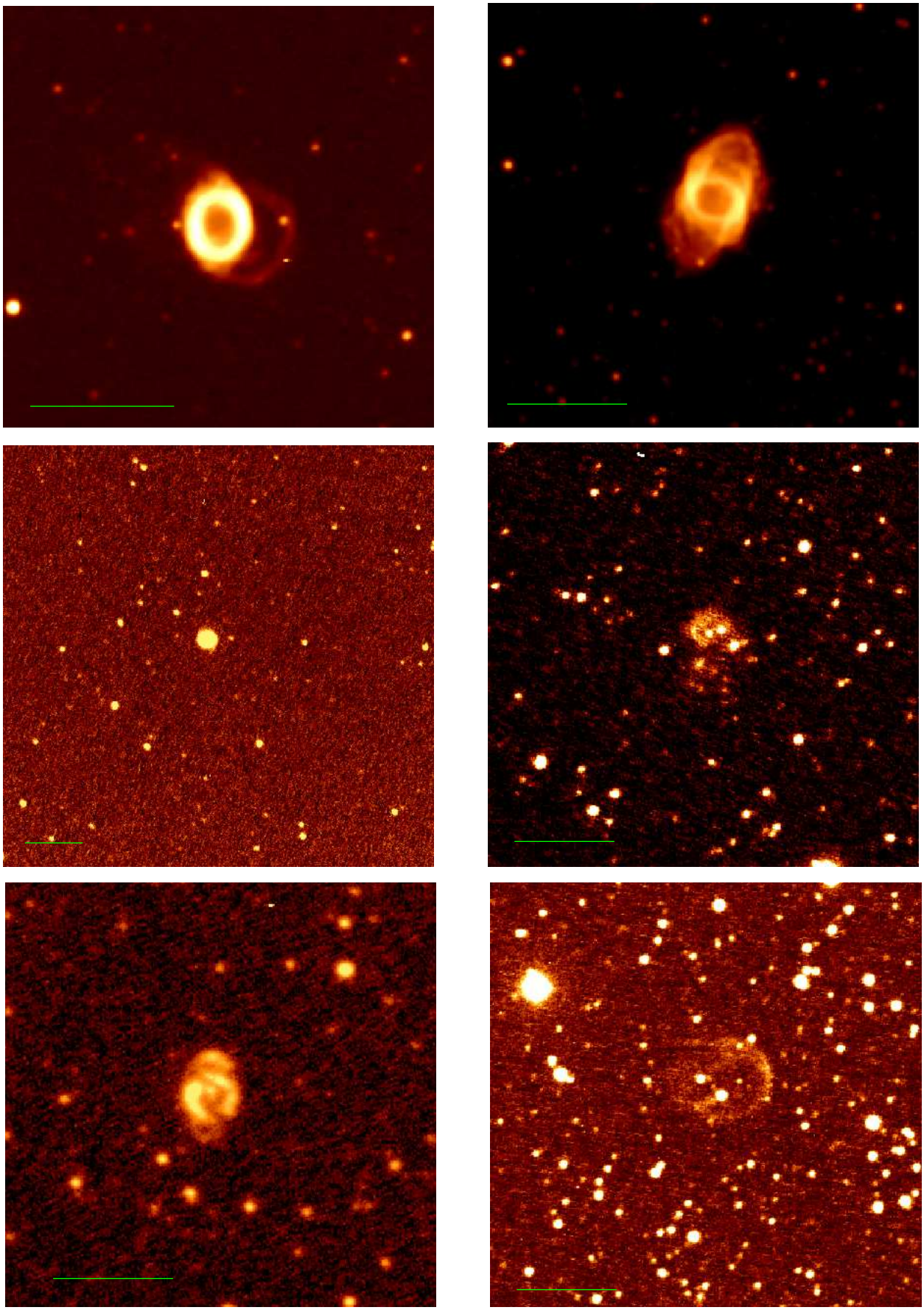

Fig. 18. Same as Fig. 3, top He 2−120 (L) and Mz 1 (L), middle He 2−163 and He 2−146, bottom Mz 2 (L) and PHR1557−5128.

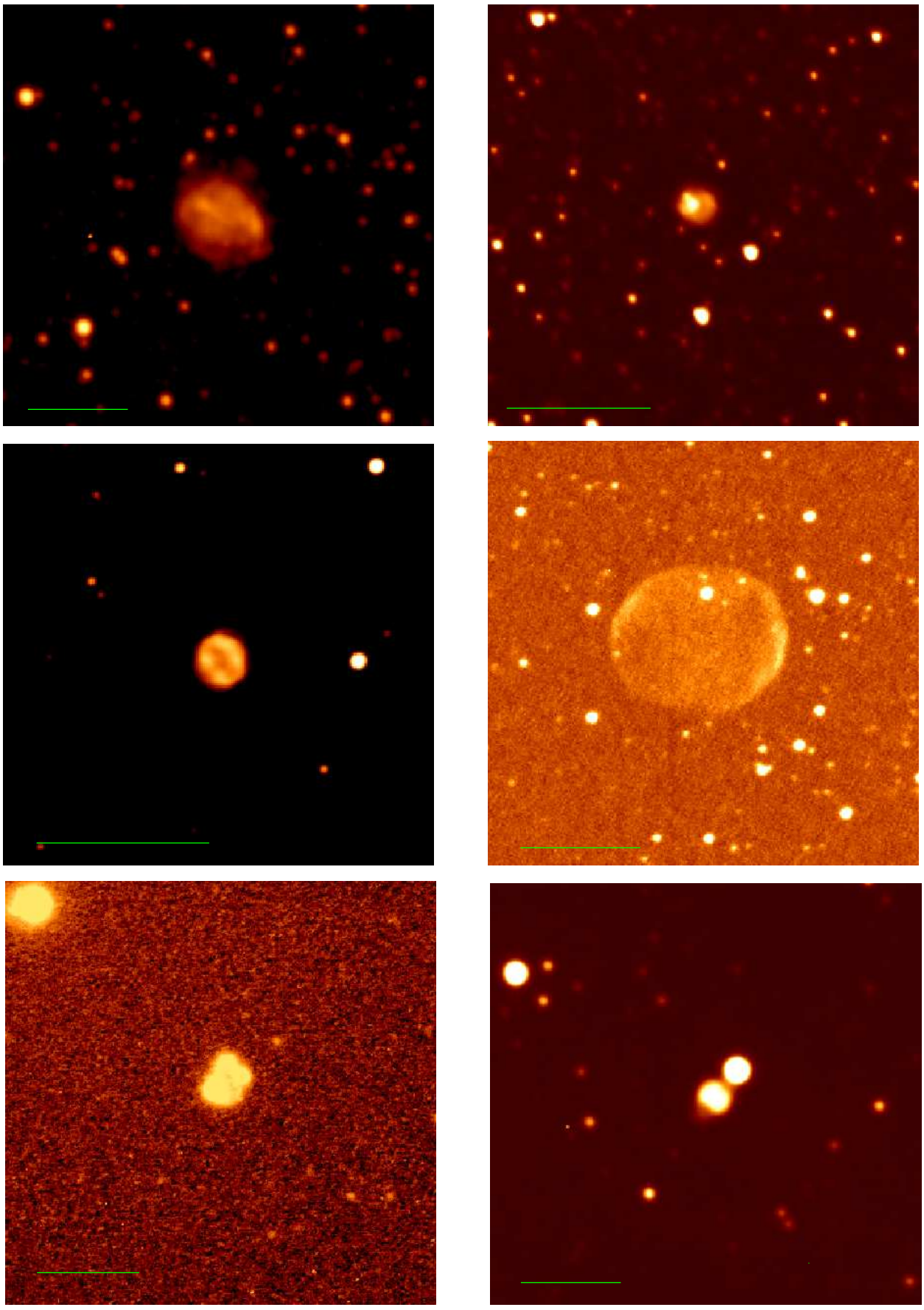

Fig. 19. Same as Fig. 3, top He 2−165 (L) and He 2−164, middle IC 4642 (L) and Lo 12, bottom NGC 6153 and H 1−3.

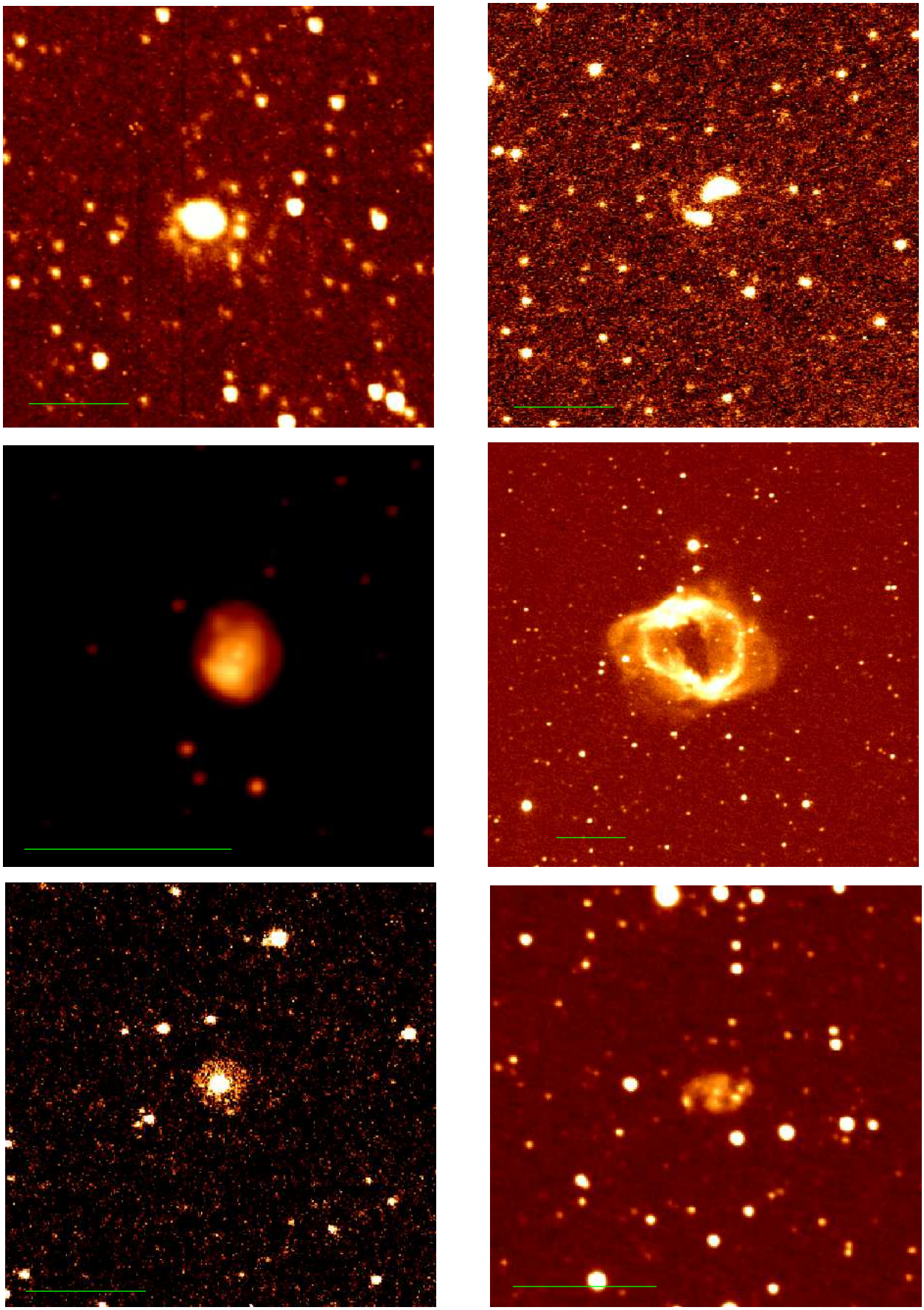

Fig. 20. Same as Fig. 3, top Pe 1−8 (L) and He 2−207, middle IC 4637 (L) and K 1−3, bottom K 2−16 (L) and Wray 16−411.

Corradi, R. L. M., Sánchez-Blázquez, P., Mellema, G., Giammanco, C., & Schwarz, H. E. 2004, A&A, 417, 637
Corradi, R. L. M., Schönberner, D., Steffen, M., & Perinotto, M. 2003, MNRAS, 340, 417
Corradi, R. L. M. & Schwarz, H. E. 1993a, A&A, 278, 247
Corradi, R. L. M. & Schwarz, H. E. 1993b, A&A, 273, 247
Corradi, R. L. M. & Schwarz, H. E. 1995, A&A, 293
Drew, J. E., Gonzalez-Solares, E., Greimel, R., et al. 2014, MNRAS, 440, 2036
Dufour, R. J. 1984, ApJ, 287, 341
Durand, S., Acker, A., & Zijlstra, A. 1998, A&AS, 132, 13
Eather, R. H. & Reasoner, D. L. 1969, Appl. Opt., 8, 227
Fredrick, L. W. & West, R. M. 1984, A&AS, 56, 325
Frew, D. J., Bojičić, I. S., Parker, Q. A., et al. 2014, MNRAS, 440, 1080
Gonçalves, D. R., Corradi, R. L. M., & Mampaso, A. 2002, in Revista Mexicana de Astronomia y Astrofisica Conference Series, Vol. 13, Revista Mexicana de Astronomia y Astrofisica Conference Series, ed. W. J. Henney, W. Steffen, L. Binette, & A. Raga, 119–122
Górny, S. K., Schwarz, H. E., Corradi, R. L. M., & Van Winckel, H. 1999, A&AS, 136, 145
Gorny, S. K., Stasińska, G., & Tylenda, R. 1997, A&A, 318, 256
Goudis, G. & Meaburn, J. 1978, A&A, 62, 283
Greve, A. & van Genderen, A. M. 1987, A&A, 174, 243
Guerrero, M. A., Toalá, J. A., Medina, J. J., et al. 2013, A&A, 557, A121
Hajian, A. R., Balick, B., Terzian, Y., & Perinotto, M. 1997, ApJ, 487, 304
Hajian, A. R., Movit, S. M., Trofimov, D., et al. 2007, ApJS, 169, 289
Hamuy, M., Suntzeff, N. B., Heathcote, S. R., et al. 1994, PASP, 106, 566
Hartl, H. & Weinberger, R. 1987, A&AS, 69, 519
Hoogerwerf, R., Szentgyorgyi, A., Raymond, J., et al. 2007, ApJ, 670, 442
Hua, C. T., Dopita, M. A., & Martinis, J. 1998, A&AS, 133, 361
Huggins, P. J., Forveille, T., Bachiller, R., & Cox, P. 2000, ApJ, 544, 889
Jones, D., Boffin, H. M. J., Miszalski, B., et al. 2014, A&A, 562, A89
Kaler, J. B., Shaw, R. A., Feibelman, W. A., & Lutz, J. H. 1989, ApJS, 70, 213
Kerber, F., Furlan, E., Roth, M., Galaz, G., & Chanamé, J. C. 2000, PASP, 112, 542
Lee, T.-H., Lim, J., & Kwok, S. 2007a, ApJ, 665, 341
Lee, T.-H., Stanghellini, L., Ferrario, L., & Wickramasinghe, D. 2007b, AJ, 133, 987
Liu, X.-W., Storey, P. J., Barlow, M. J., et al. 2000, MNRAS, 312, 585
Longmore, A. J. & Tritton, S. B. 1980, MNRAS, 193, 521
López, J. A. 2000, in Revista Mexicana de Astronomia y Astrofisica Conference Series, Vol. 9, Revista Mexicana de Astronomia y Astrofisica Conference Series, ed. S. J. Arthur, N. S. Brickhouse, & J. Franco, 201–209
López, J. A., Falcón, L. H., Ruiz, M. T., & Roth, M. 1989, in IAU Symposium, Vol. 131, Planetary Nebulae, ed. S. Torres-Peimbert, 179
Lopez, J. A., Falcon, L. H., Ruiz, M. T., & Roth, M. 1991, A&A, 241, 526
Lopez, J. A., Roth, M., & Tapia, M. 1993, A&A, 267, 194
López, J. A., Steffen, W., & Meaburn, J. 1997, ApJ, 485, 697
Louise, R., Macron, A., Pascoli, G., & Maurice, E. 1987, A&AS, 70, 201
Manchado, A., Guerrero, M. A., Stanghellini, L., & Serra-Ricart, M. 1996, The IAC morphological catalog of northern Galactic planetary nebulae
Marston, A. P., Bryce, M., Lopez, J. A., Palmer, J. W., & Meaburn, J. 1998, A&A, 329, 683
Meaburn, J. & Walsh, J. R. 1989, A&A, 223, 277
Miranda, L. F., Pereira, C. B., & Guerrero, M. A. 2009, AJ, 137, 4140
Miszalski, B., Acker, A., Parker, Q. A., & Moffat, A. F. J. 2009, A&A, 505, 249
Moore, S. L. 2007, Journal of the British Astronomical Association, 117, 204
Moreno, H., Gutierrez-Moreno, A., & Torres, C. 1991, PASP, 103, 275
Moreno, H., Gutiérrez-Moreno, A., Torres, C., & Wenderoth, E. 1987, Rev. Mexicana Astron. Astrofis., 14, 520
O'Dell, C. R., Balick, B., Hajian, A. R., Henney, W. J., & Burkert, A. 2002, AJ, 123, 3329
Palmer, J. W., Lopez, J. A., Meaburn, J., & Lloyd, H. M. 1996, A&A, 307, 225
Parker, Q. A., Phillipps, S., Pierce, M. J., et al. 2005, MNRAS, 362, 689
Pascoli, G. 1990, A&A, 232, 184
Peimbert, M. & Torres-Peimbert, S. 1983, in IAU Symposium, Vol. 103, Planetary Nebulae, ed. D. R. Flower, 233–241
Pereyra, M., Richer, M. G., & López, J. A. 2013, ApJ, 771, 114
Perinotto, M. & Corradi, R. L. M. 1998, A&A, 332, 721
Perinotto, M., Purgathofer, A., Pasquali, A., & Patriarchi, P. 1994, A&AS, 107
Phillips, J. P. 2003, MNRAS, 344, 501
Phillips, J. P. & Reay, N. K. 1983, A&A, 117, 33
Pogge, R. W. 1992, in Astronomical Society of the Pacific Conference Series, Vol. 23, Astronomical CCD Observing and Reduction Techniques, ed. S. B. Howell, 195
Polcaro, V. F., Rossi, C., Viotti, R., & Norci, L. 1997, A&A, 318, 571
Pottasch, S. R., Mo, J.-E., & Dennefeld, M. 1986, A&A, 155, 397
Rauch, T., Köppen, J., Napiwotzki, R., & Werner, K. 1999, A&A, 347, 169
Reay, N. K., Atherton, P. D., & Taylor, K. 1984, MNRAS, 206, 71
Richer, M. G., McCall, M. L., & Martin, P. G. 1991, ApJ, 377, 210
Sabin, L., Vázquez, R., López, J. A., García-Díaz, M. T., & Ramos-Larios, G. 2012, Rev. Mexicana Astron. Astrofis., 48, 165
Saurer, W. & Weinberger, R. 1987, A&AS, 69, 527
Schwarz, H. E. 1992, A&A, 264, L1
Schwarz, H. E., Corradi, R. L. M., & Melnick, J. 1992, A&AS, 96, 23
Smith, L. J., Crowther, P. A., & Prinja, R. K. 1994, A&A, 281, 833
Smith, N., Bally, J., & Walawender, J. 2007, AJ, 134, 846
Stahl, O. 1987, A&A, 182, 229
Stanghellini, L., Corradi, R. L. M., & Schwarz, H. E. 1993a, A&A, 279, 521
Stanghellini, L., Corradi, R. L. M., & Schwarz, H. E. 1993b, A&A, 276, 463
Streicher, M. 2010, Monthly Notes of the Astronomical Society of South Africa, 69, 229
Szentgyorgyi, A., Franco, J., López-Martín, L., Raymond, J. C., & Villaver, E. 2003a, in Revista Mexicana de Astronomia y Astrofisica Conference Series, Vol. 15, Revista Mexicana de Astronomia y Astrofisica Conference Series, ed. J. Arthur & W. J. Henney, 84–84
Szentgyorgyi, A., Raymond, J., Franco, J., Villaver, E., & López-Martín, L. 2003b, ApJ, 594, 874
Tweedy, R. W. & Kwitter, K. B. 1996, ApJS, 107, 255
Vázquez, R. 2012, ApJ, 751, 116
Vena Valdarenas, R. R., Schmidt, E. O., Volpe, M. G., Weidmann, W., & Mudrik, A. 2015, Boletin de la Asociacion Argentina de Astronomia La Plata Argentina, 57, 197
Walsh, A. J., Hyland, A. R., Robinson, G., & Burton, M. G. 1997, MNRAS, 291, 261
Zhang, C. Y. & Kwok, S. 1998, ApJS, 117, 341
Zuckerman, B. & Aller, L. H. 1986, ApJ, 301, 772

Table 4. List of PNe included in our atlas. The PNe are denoted by their common name and by their PN G designation. Sixth column lists the telescope used in each observation, EABA and CASLEO, indicated by "E" and "C" respectively. Seventh column lists the number of combined images and eighth column shows the figure number for each nebulae. PNe observed by Hua et al. (1998) and Balick (1987) are marked by "*" and objects labelled with "†" have probably Hα contamination or only the continuum emission is detected.

N	Name	PN G	RA (J2000)	Dec (J2000)	Telescope	Images	Figure
1	IC 5148−50*†	002.7−52.4	21 59 31.7	−39 22 36.2	E	10	3
2	Hb 4	003.1+02.9	17 41 52.7	−24 42 08.0	E	11	3
3	SaWe 3*†	013.8−02.8	18 26 03.1	−18 12 05.6	E	15	3
4	HDW 12	014.8−25.6	19 58 13.2	−26 28 15.4	C	3	3
5	DeHt 3	019.4−13.6	19 17 04.6	−18 01 34.2	E	17	3
6	A 66	019.8−23.7	19 57 31.8	−21 36 36.8	C	8	3
7	A 67	043.5−13.4	19 58 29.3	+03 02 22.6	C	3	4
8	NGC 246*	118.8−74.7	00 47 03.8	−11 52 21.6	C	3	4
9	PHR0615−0025	209.1−08.2	06 15 20.4	−00 25 49.1	C	3	4
10	K 1−11	215.6+11.1	07 36 07.7	+02 42 17.2	C	8	4
11	PHR0702−0324	217.2+00.9	07 02 34.2	−03 24 34.9	C	3	4
12	PHR0705−0924	222.9−01.1	07 05 51.4	−09 24 11.2	C	4	4
13	PHR0700−1143	224.3−03.4	07 00 05.8	−11 43 50.9	C	5	5
14	PHR0716−1053	225.4+00.4	07 16 08.0	−10 53 06.0	C	6	5
15	PHR0711−1238	226.4−01.3	07 11 43.3	−12 38 03.1	C	6	5
16	M 1−16	226.7+05.6	07 37 18.9	−09 38 48.1	E	10	5
17	PHR0719−1222	227.1+00.5	07 19 46.7	−12 22 46.9	C	3	5
18	PHR0727−1259	228.6+01.9	07 27 49.0	−12 59 30.1	C	3	5
19	PHR0727−1707	232.1−00.1	07 27 08.3	−17 07 14.2	C	5	6
20	PHR0724−1757	232.6−01.0	07 24 43.4	−17 57 51.1	C	3	6
21	SaWe 1	233.0−10.1	06 50 41.0	−22 26 09.3	C	3	6
22	HaWe 9	236.0−10.6	06 54 29.0	−25 21 11.6	C	6	6
23	PHR0730−2151	236.7−01.6	07 30 46.9	−21 51 43.9	C	3	6
24	ESO 427−19	239.6−12.0	06 55 12.1	−29 07 28.4	C	3	6
25	NGC 2610†	239.6+13.9	08 33 23.5	−16 08 55.9	E	13	7
26	PHR0726−2858	242.5−05.9	07 26 04.8	−28 58 23.5	C	4	7
27	PRTM 1	243.8−37.1	05 03 01.7	−39 45 44.0	C	3	7
28	PHR0742−3247	247.5−04.7	07 42 23.6	−32 47 44.9	C	3	7
29	A 23	249.3−05.4	07 43 18.9	−34 45 13.0	C	3	7
30	PHR0834−2819	249.8+07.1	08 34 18.1	−28 19 03.0	C	3	7
31	PHR0803−3331	250.4−01.3	08 03 12.5	−33 31 01.9	C	4	8
32	PHR0736−3901	252.4−08.7	07 36 25.2	−39 01 31.1	C	3	8
33	PHR0820−3516	253.9+00.7	08 20 52.4	−35 16 32.9	C	3	8
34	VBRC 1	257.5+00.6	08 30 58.0	−38 19 52.3	C	3	8
35	Wray 17−1	258.0−15.7	07 14 48.0	−46 57 24.4	C	3	8
36	He 2−11	259.1+00.9	08 37 08.2	−39 26 25.5	C	3	8
37	Wray 16−20	260.7−03.3	08 23 40.4	−43 12 44.0	C	3	9
38	He 2−15	261.6+03.0	08 53 30.6	−40 03 34.4	C	3	9
39	NGC 2818	261.9+08.5	09 16 00.5	−36 37 31.6	E	20	9
40	Wray 17−18	262.6−04.6	08 23 53.7	−45 31 09.9	E	10	9
41	ESO 209−15	263.3−08.8	08 05 10.9	−48 23 30.1	E	20	9
42	He 2−7†	264.1−08.1	08 11 31.9	−48 43 14.5	C	3	9
43	ESO 259−10	265.1−04.2	08 34 07.0	−47 16 38.1	C	3	10
44	PHR0911−4205	265.4+04.2	09 11 48.5	−42 05 09.9	C	4	10
45	PHR0927−4347	268.6+05.0	09 27 28.1	−43 47 53.2	C	6	10
46	PHR0905−4753	268.9−00.4	09 05 39.6	−47 53 38.0	C	3	10
47	He 2−37	274.6+03.5	09 47 24.3	−48 58 19.1	C	3	10
48	PHR0924−5506	276.1−03.3	09 24 15.1	−55 06 24.8	C	6	10
49	NGC 2899	277.1−03.8	09 27 03.5	−56 06 18.3	E	20	11
50	PHR0958−5039	277.1+03.3	09 58 10.2	−50 39 34.9	C	6	11
51	Wray 17−31	277.7−03.5	09 31 27.1	−56 17 41.1	E	20	11
52	He 2−32	278.5−04.5	09 30 55.9	−57 36 57.8	C	3	11
53	PHR0940−5658	279.1−03.1	09 40 52.5	−56 58 00.1	C	3	11
54	PHR1010−5146	279.2+03.5	10 10 04.1	−51 46 48.0	C	6	11
55	He 2−36	279.6−03.1	09 43 26.0	−57 16 59.7	E	10	12
56	Ste 2−1	280.0+02.9	10 11 57.9	−52 38 15.2	C	3	12
57	PHR1019−6059	285.5−03.3	10 19 27.6	−60 59 09.9	C	3	12

Table 4. continued.

N	Name	PN G	RA (J2000)	Dec (J2000)	Telescope	Images	Figure
58	PHR1036−5909	286.3−00.7	10 36 09.2	−59 09 20.2	C	6	12
59	He 2−55	286.3+02.8	10 48 43.1	−56 03 23.0	E	14	12
60	PHR1046−6109	288.4−01.8	10 46 51.1	−61 09 23.0	C	3	12
61	Hf 38	288.4+00.3	10 54 34.9	−59 09 48.7	C	3	13
62	PHR1058−5853	288.7+00.8	10 58 02.9	−58 53 34.1	C	3	13
63	Hf 39	288.9−00.8	10 53 58.9	−60 26 42.0	E	3	13
64	Hf 48*	290.1−00.4	11 03 55.6	−60 36 05.6	E	20	13
65	Fg 1	290.5+07.9	11 28 35.9	−52 56 06.4	E	10	13
66	NGC 3699*	292.6+01.2	11 27 59.2	−59 57 32.0	C	3	13
67	He 2−70*	293.6+01.2	11 35 12.6	−60 16 54.1	C	3	14
68	BlDz 1	293.6+10.9	11 53 03.8	−50 50 41.8	E	25	14
69	NGC 3918	294.6+04.7	11 50 18.9	−57 10 51.4	E	20	14
70	He 2−72*	294.9−00.6	11 41 37.9	−62 28 56.9	C	3	14
71	NGC 3195	296.6−20.0	10 09 22.0	−80 51 30.6	E	10	14
72	He 2−76	298.2−01.7	12 08 26.0	−64 12 12.1	E	13	14
73	PHR1221−5907	299.0+03.5	12 21 00.7	−59 07 32.9	C	4	15
74	K 1−23	299.0+18.4	12 30 52.0	−44 14 22.2	E	20	15
75	Wray 16−121	302.6−00.9	12 48 31.1	−63 49 56.5	C	3	15
76	PHR1250−6346	302.7−00.9	12 50 04.4	−63 46 51.9	E	14	15
77	Wray 16−122	304.2+05.9	13 00 41.4	−56 53 28.3	C	6	15
78	NGC 5189*	307.2−03.4	13 33 41.9	−65 58 28.9	E	20	15
79	He 2−99	309.0−04.2	13 52 31.0	−66 23 28.0	E	19	16
80	VBRC 5	309.2+01.3	13 43 59.2	−60 49 40.4	C	3	16
81	He 2−103	310.7−02.9	14 05 36.9	−64 40 57.0	E	20	16
82	LoTr 7	310.8−05.9	14 15 23.1	−67 31 57.6	E	14	16
83	PHR1408−6229	311.7−00.9	14 08 47.3	−62 29 57.8	C	3	16
84	He 2−111	315.0−00.3	14 33 18.3	−60 49 44.6	E	14	16
85	He 2−119*	317.1−05.7	15 10 39.9	−64 40 19.1	E	20	17
86	VBRC 6	317.8+03.3	14 41 35.7	−56 15 06.6	E	25	17
87	He 2−114	318.3−02.0	15 04 08.8	−60 53 21.2	E	20	17
88	He 2−116	318.3−02.5	15 06 00.8	−61 21 24.4	E	10	17
89	ESO 135−04	318.4−03.0	15 08 42.8	−61 44 03.9	E	20	17
90	IC 4406*	319.6+15.7	14 22 26.5	−44 09 06.0	E	10	17
91	He 2−120	321.8+01.9	15 11 56.1	−55 39 51.1	E	10	18
92	Mz 1	322.4−02.6	15 34 16.7	−59 08 59.5	E	10	18
93	He 2−163	327.8−07.2	16 29 30.3	−59 09 22.3	E	12	18
94	He 2−146	328.9−02.4	16 10 40.9	−54 57 31.9	E	20	18
95	Mz 2	329.3−02.8	16 14 32.1	−54 57 04.0	E	20	18
96	PHR1557−5128	329.7+01.4	15 57 07.4	−51 28 00.8	E	20	18
97	He 2−165	331.5−03.9	16 29 59.6	−54 09 36.7	E	12	19
98	He 2−164	332.0−03.3	16 29 53.2	−53 23 04.1	E	14	19
99	IC 4642	334.3−09.3	17 11 45.4	−55 24 02.4	E	10	19
100	Lo 12	340.8+10.8	16 08 26.3	−37 08 48.3	E	20	19
101	NGC 6153	341.8+05.4	16 31 30.9	−40 15 22.5	E	14	19
102	H 1−3	342.7+00.7	16 53 31.5	−42 39 18.1	E	10	19
103	Pe 1−8	342.9−02.0	17 06 22.8	−44 13 12.1	E	10	20
104	He 2−207	342.9−04.9	17 19 32.5	−45 53 10.0	E	18	20
105	IC 4637	345.4+00.1	17 05 09.0	−40 52 57.1	E	10	20
106	K 1−3*	346.9+12.4	16 23 17.3	−31 44 56.9	E	12	20
107	K 2−16†	352.9+11.4	16 44 49.1	−28 04 05.4	E	17	20
108	Wray 16−411	353.7−12.8	18 26 41.5	−40 29 51.1	E	14	20